THESIS FOR THE DEGREE OF DOCTOR OF PHILOSOPHY

Bacteria-responsive materials for drug delivery

MARINA CRAIG

Department of Chemistry and Chemical Engineering
CHALMERS UNIVERSITY OF TECHNOLOGY
Gothenburg, Sweden 2015

Cover: Microcapsules loaded with antimicrobial drugs are assembled using template assisted assembly and the layer-by-layer technique. The capsules' nanofilm shell is designed to stay intact if no infection is present. However, if the surface is covered with bacteria, the capsule structure ruptures and exposes the drug. Photo credit (*Staphylococcus aureus*): Dr. Dennis Kunkel.

Bacteria-responsive materials for drug delivery

MARINA CRAIG

Department of Applied Surface Chemistry
Chemistry and Chemical Engineering
Chalmers University of Technology

ABSTRACT

The number of diabetics, obese individuals and other patients carrying other lifestyle diseases is increasing worldwide. At the same time the population is ageing. These patients all suffer from poor blood circulation, which often gives rise to non-healing, or chronic, wounds. Thus, the number of chronic wounds is also increasing at a fast pace. Such wounds often carry infection since the wound environment is favorable for bacteria. The wounds cause pain, odor and can lead to amputation or even death. Hence, the patients are treated with systemic and topical antimicrobial substances, *e.g.* antibiotics. However, the overexposure and misuse of such drugs has created another issue worldwide: bacterial resistance. There are already some infections that are difficult to treat due to the rapid development of bacterial resistance and fewer working drugs.

Our work has focused on a release platform that can administer drugs only when a wound shows signs of infection. By sensing the type of infection at hand, the release system should break down and expose a suitable antimicrobial substance to the bacteria. Such a release system would not only combat the infection but also decrease the risk of bacterial resistance and other side effects on the patient, since it would be administered locally and only when it is needed.

Two bacteria were chosen as targets, *Staphylococcus aureus* and *Pseudomonas aeruginosa*, which often are pathogenic in chronic wounds. Both bacteria exude very substrate specific proteases, *i.e.* V8 and Protease IV, respectively. Hence, nanofilms corresponding to each protease were assembled via the layer-by-layer route. V8 readily degrades peptide bonds involving poly-L-glutamic acid (PLGA), which also was the main component in the release system against *S. aureus*, while Protease IV degrades bonds involving poly-L-lysine, which hence was used as component in the release system against *P. aeruginosa*. The nanofilms were found not to be degraded by normal human enzymes; however, each bacterial protease ruptured their respective film if they reached a concentration similar to the concentration found in a chronic wound. Consequently, the drug was released or exposed only when in contact with the bacterial enzymes. Such release systems could be used to fight infection while avoiding bacterial resistance and misuse of antimicrobials.

Keywords: Layer-by-layer, multilayer, enzymatic degradation, triggered release, controlled release, nanofilm, infection

LIST OF PAPERS

I.   **Polypeptide multilayer self-assembly and enzymatic degradation on tailored gold surfaces**

Marina Craig, Romain Bordes, Krister Holmberg

Soft Matter **2012**, *8* (17), 4788.

II.   **Polypeptide multilayer self-assembly studied by ellipsometry**

Marina Craig, Krister Holmberg, Eric Le Ru, Pablo Etchegoin

J Drug Delivery **2014**, *vol. 2014*, ID 424697, 5 pages.

III.   **Bacterial protease triggered release of biocides from microspheres with an oily core**

Marina Craig, Mona Amiri, Krister Holmberg

Colloids and Surfaces B: Biointerfaces **2015**, *127*, 200.

IV.   **Biodegradable nanofilms on microcapsules for controlled release of drugs to infected chronic wounds**

Marina Craig, Erich Schuster, Krister Holmberg

Materials Today Proceedings **2015**, *2*, 118.

V.   **Bacteria-triggered degradation of nanofilm shells for release of antimicrobial agents**

Marina Craig, Annika Altskär, Lars Nordstierna, Krister Holmberg

Under revision for Materials Chemistry B

CONTRIBUTION LIST

I.   Responsible for all experimental work and most of the data analysis. Responsible for writing the manuscript.

II.   Responsible for all experimental work and the data analysis. Responsible for writing the manuscript.

III.   Responsible for planning materials, methods and for the data analysis. Responsible for writing the manuscript.

IV.   Responsible for all sample preparations and some data analysis. Responsible for writing the manuscript.

V.   Responsible for all sample preparations and some data analysis. Responsible for writing the manuscript.

Table of Contents

x

Bacteria-responsive materials for drug delivery

1 INTRODUCTION

Diabetes, obesity and cardiovascular disease are factors that often lead to the development of chronic wounds. Even though millions of people suffer from chronic wounds there is not a straightforward answer to why the healing process is disturbed, but poor blood circulation is almost always a common factor. Complications connected to the prolonged healing time are not only costly, they also create suffering for the patient due to increased pain, infection, sepsis, amputation and even death. Approximately 2% of the general population in the US suffers from chronic wounds and the estimated cost exceeds US$ 50 billion (*Kuhn 1992, Gordon 2004, Hess 2004, Sen 2009, Driver 2010*). As for the future, the prevalence of hard-to-heal wounds will rise due to the dramatic increase of metabolic disorders in the world. For example, it is predicted that approximately 8.3% of all adults had diabetes in 2013, *i.e.* 382 million people where almost 50% were undiagnosed (The international diabetes federation). In the year 2035 the number of diabetics is estimated to 592 millions, which is an astonishing 55% increase from 2013. A lifestyle change in all types of patients is needed to increase blood circulation; however, age, pain and the will to change at an early stage are factors that prevent healing. Thus, the prevention and treatment of wounds becomes a necessary component for the management of the underlying disease. This work describes bacteria-responsive drug delivery to chronic wounds that carry infection.

1.1 Background

1.1.1 Chronic wounds

Patients with diabetic foot ulcers (DFU), venous leg ulcers (VLU) and pressure ulcers (PU) all have poor circulation, which desensitizes the patient's extremities, *e.g.* lower leg or foot regions for DFU due to microvascular damage (*Jarrod 2011*). This loss of sensation makes it difficult to discover the wound as it appears, allowing it to spread and stay untreated until a large wound has been established. Daily checks of the patient's skin are hence crucial. Also, the lack of blood supply promotes swelling and oedema, particularly in VLU patients due to the increased venous pressure. The insufficient circulation interrupts the patient's normal healing process and a chronic wound appears. Other factors that contribute to chronic wounds can be neuropathy and difficulty moving. Cancer patients with radiation treatment, as well as burn victims, are also more prone to develop hard-to-heal wounds, often in combination with a bacterial infection.

The normal wound healing process is traditionally divided into three phases: **the inflammation phase**, **the proliferative phase** and **the maturation and remodeling phase** (*Velnar 2009, Beanes 2003*), see Figure 1.1. The inflammation phase is the first stage and describes the wound as it appears and the short time after the skin has been broken. Hemostasis is initiated by the clotting cascade, *i.e.* the bleeding prevention mechanism called coagulation. Different chemical substances when dead cells excrete certain chemicals, which in turn results in release of additional pro-inflammatory substances. Blood vessels dilate and allows for release of wound fluid, thus increasing the temperature and the microcirculation in the affected area. Simultaneously, a temporary extracellular matrix (ECM) is built up as support in the healing wound. The duration of the inflammatory phase varies; however, it lasts until the wound is properly "cleaned".

The phases of cutaneous wound healing

Expert Reviews in Molecular Medicine©2003 Cambridge University Press
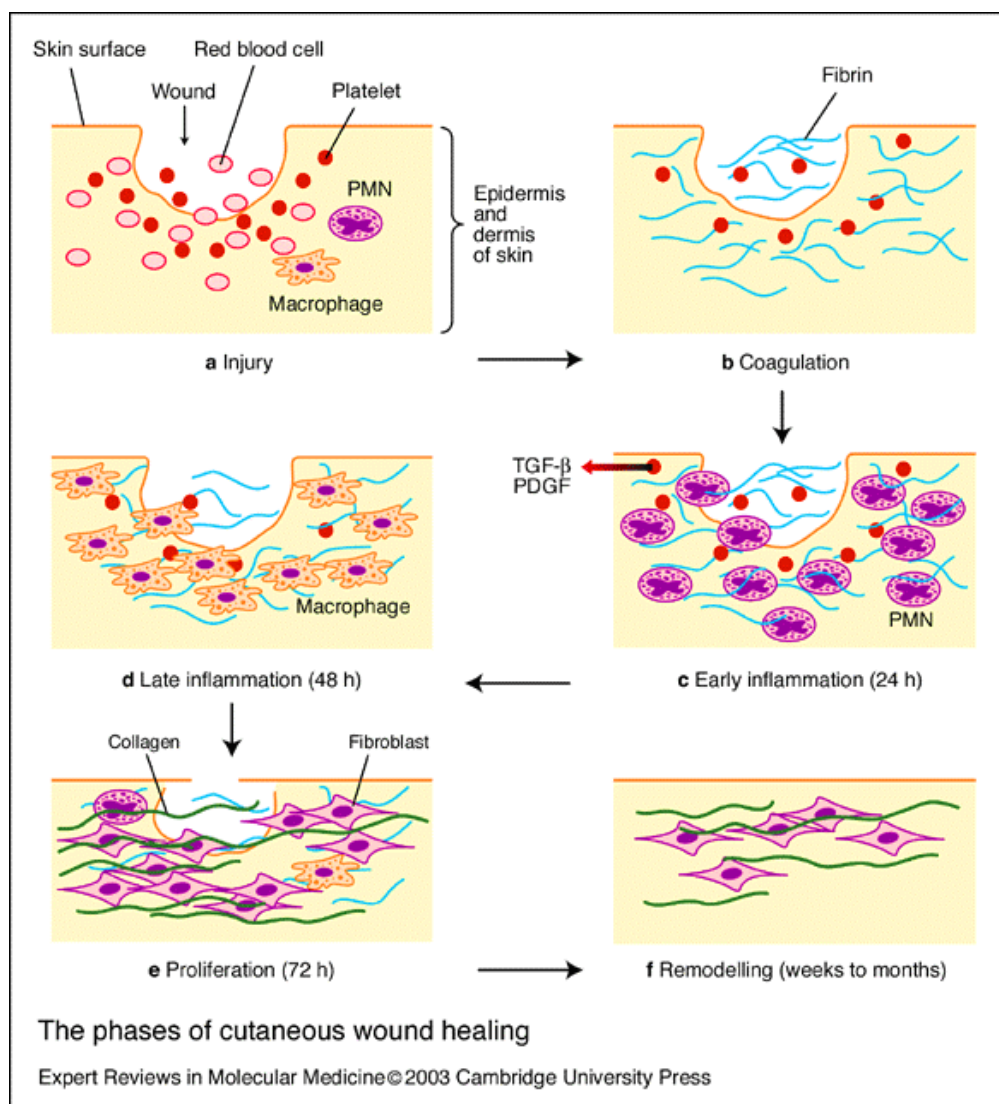
and growth factors are then released to attract inflammatory cells, which not only excrete pro-inflammatory cytokines and proteases, but also through phagocytosis clean the wound from foreign matter such as bacteria and dead tissue. Pain develops

Figure 1.1 *The three different stages in normal wound healing; the complex inflammatory phase in (a), (b), (c) and (d), the proliferative phase in (e), and the maturation and remodeling phase in (f). (Cambridge University Press, 2003)*

2

In the proliferative phase several growth factors are exuded to allow for tissue to be restored. Fibroblasts, endothelial cells and other new cells gradually replace the inflammatory cells as the healing proceeds. At the same time angiogenesis, or development of new blood vessels, is triggered. Granulation tissue then builds up the deeper regions of the wound when fibroblasts produce collagen. Also epithelialization and contraction of the wound will start during the proliferative stage, which normally lasts for a few weeks depending on the state of the wound. The third and last stage, the maturing and remodeling phase, involves degradation and replacement of the temporary ECM built during the inflammatory stage. The permanent ECM stores collagen which is assembled in bundles that make up the scar tissue.

In a chronic wound the normal healing cascade is interrupted. The underlying causes for a hard-to-heal wound may create an inflammatory environment that triggers the production of proteases degrading the ECM, hence degrading the wound faster than the normal wound healing process is able to rebuild the wound. Also, DFU and VLU patients may have a slow and inadequate production of the permanent ECM and the following epithelialization, which also will result in stalled healing. In other words, the balance between degrading and producing molecules is of utmost importance for wound healing. Due to the disordered healing environment, bacterial infection is common in chronic wounds (*Bowler 1998, Landis 2008*) and results in a high amount of bacterial proteases (*Greener 2005*). The infection and the foreign matter it brings stalls the healing further and allows for additional degradation of tissue and spreading of the wound. Such an infection is normally treated with oral antibiotics or with gels, creams or wound dressings containing antimicrobial substances (*Burell 2003*). The above agents are usually applied in excess and may generate resistant bacteria (*Flattau 2008, Percival 2008*) and cause damage on the patient's own cells, hence prolonging the healing time and the suffering for the patient and increasing the treatment cost. With "intelligent" delivery of the active substance, *i.e.* optimized timing and dosage, resistant bacteria can be avoided and wound healing triggered.

Within chronic wound care, the primary and very important function of a dressing is to absorb and retain wound exudate. Materials used for this purpose include nonwovens, polyurethane foams, hydrogels, *etc.*, often with a wound contact layer that prevents the absorbing material to stick to the wound. A secondary function of a wound dressing can be to serve as a reservoir for a bioactive substance that promotes wound healing and which is released into the wound on demand. It is obviously of utmost importance to treat the underlying cause of the chronic wound; however, the immediate danger lies in an untreated and often infected wound, which could lead to severe outcomes such as amputation or even death.

1.1.2 Wounds and treatments

The earliest wound treatments and dressings were natural materials and liquids, such as leaves, milk, grease, and mixtures of whatever people thought would heal a wound. Later on, to protect and absorb wound exudate, gauze was used. Originally gauze was made of silk, but it changed to cotton when it was

possible to weave it into loose, net-like fabrics for wound care purposes. However, even though gauze easily absorbs exudate and to some extent protects the wound, it also sticks to the wound surface and grows into the scab that forms on the healed wound. As a result, the wound dressing change will damage the skin that already has healed and the wound will resurface.

Since the discovery of moist wound healing, there has been a constant flow of new dressing materials and wound dressings on the market. More complex dressings consisting of several layers of top, core and wound facing interfaces have been invented consisting of *e.g.* nonwovens, polyurethane foams, hydrocolloids, hydrogels and soft silicones. From the 1990's until today, other forms of treatments were also introduced, such as antimicrobial dressings containing silver in different forms, collagen dressings, negative pressure therapy, bioengineered tissue dressings and dressings or skin substitutes containing pharmaceuticals, growth factors or other active substances. The myriad of treatments and dressings makes it difficult to choose the product that suits the patient best. Initially the material needs to absorb and retain wound exudate, a property that cannot be compromised. Further, the wound contact layer should provide moist wound healing, and it should prevent the layer from sticking to the wound.

Now, when the chronic wound is given a favorable environment for healing, additional treatment can be added. Active substances to promote healing could be the trigger needed for the wound to start the stalled healing cascade, especially if the wound is infected. An antimicrobial that is released only when an infection is present

would be the ultimate. Human cells should preferably not get exposed to such substances due to their aggressive nature towards all living cells. Also, if only released when an active infection is present, then the risk of resistance is reduced.

In this research project a hydrophilic nonwoven material was chosen as substrate for *2D* nanofilm formation. This type of material is commonly used for wound care, either as an absorbing wound material in direct contact with the wound, or as part of the absorbing core of a complex dressing, see Figure 1.2. Additionally, the concept was developed into a *3D* version including microspheres and microcapsules containing antimicrobial substances.

Exudate path in a dressing
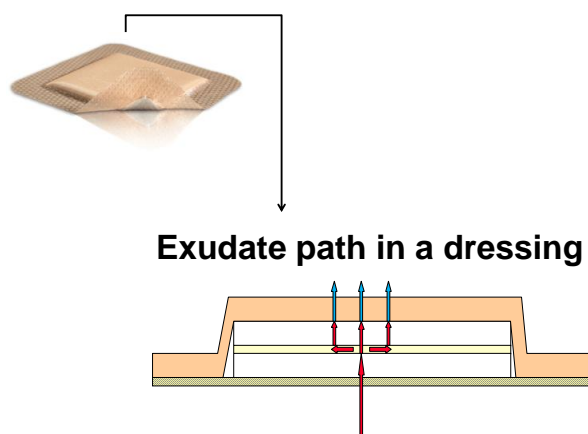
Figure 1.2 *A complex dressing and its wound exudate path. The dressing absorbs wound exudate through the wound contact layer and the liquid is then transported to the first core material by capillary forces. Retention is an important property, which means spreading and holding the liquid, and is important between the first and the second core material, as well as inside the second core. The next step is transport of water vapor through the backing film of the wound dressing. Nonwoven is a commonly used material in the core of such dressings. (Mölnlycke Health Care AB)*

2 OBJECTIVES

Triggered, controlled or targeted release are some of the current "buzz words" when it comes to drug delivery. Consequently, self-assembled thin films have become an increasingly popular research topic in the last decade when acting as a barrier in drug release. Unnecessary exposure of active substances and pharmaceuticals has raised problems such as resistant bacteria, resistant cancer cells and different side effects ranging from light to severe. Avoiding treating the whole body, but instead targeting the affected areas, as well as treating the patient only when the drug is needed, would ease the current problem of overexposure. Additionally, the thin film acts as a barrier and can prolong the lifetime of a drug or enhance the therapeutic effect, *e.g.* help bypassing cancer cells' defense systems (*Poon 2011*). Films in the nanometer range, "nanofilms", can be prepared by the layer-by-layer (LbL) technique, which involves alternating deposition of oppositely charged polyelectrolytes onto a surface of choice, a procedure pioneered by Decher (*Decher 1992, Decher 1997*).

In this work, polyelectrolytes were assembled using the LbL technique to form either *2D* or *3D* nanofilm structures. The *2D* version was deposited on a tailored gold surface resembling a traditional nonwoven wound dressing material. The *3D* versions were either microspheres assembled via the o/w emulsion pathway or microcapsules made through template assisted assembly. All versions were made with the intention to be degraded by bacterial proteases while remaining intact in absence of such proteases. Such systems could thus carry an antimicrobial drug and release the active substance upon a trigger exuded by the bacteria. The choice of polyelectrolytes acting as shell was hence key. As for *Staphylococcus aureus* and *Pseudomonas aeruginosa*, particularly virulent strains, proteases that degrade host tissue for nutritional use during infection were investigated. Also, the specificity of the proteases was considered, since the drug release should be directly dependent on the amount of bacterial enzymes at the infected site, *e.g.* a chronic wound. *S. aureus* proved to have a glutamic acid-bond specific endoprotease filling the right criteria, and *P. aeruginosa* a lysine-bond specific one. Tuning the release of actives to the degree of infection seems not to have been described before, although antimicrobial LbL films have been reported (*Shukla 2010*). Quartz crystal microbalance with dissipation monitoring (QCM-D) was used as the main method for studying the stepwise *2D* nanofilm LbL assembly followed by the enzymatic degradation at physiological pH. The microspheres were studied with a zetasizer and confocal laser scanning microscopy (CLSM), while UV/vis was used for the release studies. As for the microcapsules, a zetasizer, CLSM, fluorescence microscopy, NMR and antimicrobial tests were used when investigating the build-up, drug loading and enzymatic degradation. This thesis describes the use of currently available building stones that are assembled for "intelligent" release of drugs to infected wounds.

3 THEORY

3.1 Polyelectrolytes

Polyelectrolytes are polymers with ionizable groups, such as carboxylates or protonated amines, and are normally easily dissolved in water and other polar solvents. The polyelectrolyte can either carry a net negative or a net positive charge, *i.e.* be an anionic or a cationic polyelectrolyte. If the polymer has strongly dissociating groups, the charge is not pH dependent. Such molecules are called strong polyelectrolytes. On the other hand, a weak polyelectrolyte has reversible proton transfer and hence the charge will change with pH (*Holmberg 2003, Malmsten 2003*). Polyelectrolytes may also exhibit a more complex structure, either have charges that are unevenly distributed over the macromolecule or be a polyampholyte that carries both negative and positive charges. Proteins are examples of polyampholytes (*Fleer 1993*).

When in solution, the dissociated groups are accompanied by counterions of opposite charge. These counterions should not be mistaken for the ionic strength of the solution, which describes the added amount of salt, which is an important parameter for tuning the solution properties of polyelectrolytes (*Decher 2003, Dobrynin 2005*). The immediate proximity of counterions increases the osmotic pressure of the solution and contributes to the polyelectrolytes' solubility in water (*Takahashi 1970, Netz 2007, Nagy 2010*). In a dilute polyelectrolyte solution and at low ionic strength, the macromolecule is in its most extended form, primarily due to intramolecular forces. Each of the charged repeating units of the macromolecule experiences repulsion and the forces are

strongest in the center of the molecule (*Dobrynin 2005*). The extended and swollen form of the polyelectrolyte influences the overlap concentration, making it very small. Due to these particular properties of polyelectrolytes, the viscosity is also often larger than for uncharged polymers of similar molecular weight and of the same concentration (*Netz 2007*). As the ionic strength increases, the charged polymeric molecule changes conformation into a blob-like, coiled structure, see Figure 3.1. This effect is due to screening of the charges. Other parameters that affect polyelectrolytes are pH, temperature, concentration and solvent composition (*Dubas 1999, Decher 2003, Dobrynin 2005*).
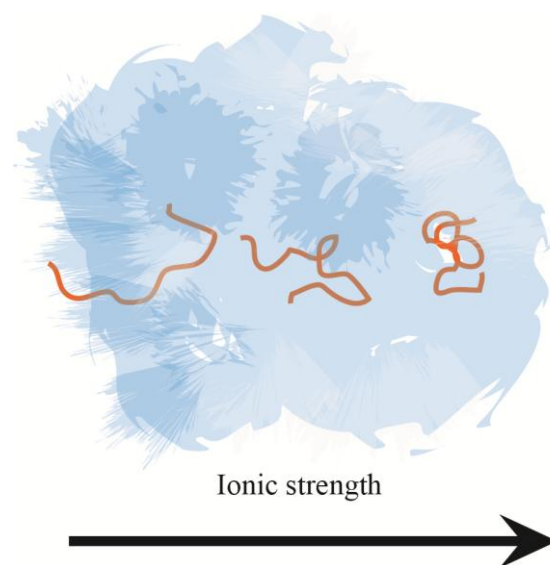
Figure 3.1 *Polyelectrolytes in solution and their conformational dependence on ionic strength. With increasing salt concentration and at low poly-electrolyte concentration the polyelectrolyte's charges are increasingly screened, which allows the polymer to form a more coil-like structure.*

3.1.1 Multilayer formation and layer-by-layer

Until around 2000 the Langmuir-Blodgett (LB) technique was the most common method for preparing nanostructured films. The technique is based on the transfer of a

monolayer formed on a water surface to a solid surface (*Blodgett 1934, Blodgett 1937*). However, the LB technique has its limitations, since it requires very hydrophobic molecules, and the films may rearrange after and during the transfer to the solid surface. The layer-by-layer (LbL) film forming technique was pioneered by Decher in the early 1990's (*Decher 1992, Decher 1997*), creating a scientific platform for multilayer formation that commercially caught up speed ten years later. LbL enables simple nanofilm assembly and has a wide range of (potential) applications.

LbL deposition belongs to the same category as LB, *i.e.* template assisted assembly. However, LbL is a swift technique with less uncertain outcome than LB. Without significant chemical modification, tailored multilayers can be assembled from a variety of components (*Lvov 1994, Sukhorukov 1996*). The assembly of LbL films relies on an overcompensated surface charge when an oppositely charged polyelectrolyte is deposited onto it, *i.e.* sequential deposition of oppositely charged polyelectrolytes can be performed if the surfaces have an excess opposite charge. The assembly requires a rinsing step before the oppositely charged polyelectrolyte can be deposited. This procedure can be repeated many times, see Figure 3.2. The adsorption of polyelectrolytes can be carried out on a variety of different surfaces, as long as the surface has a charge opposite to that of the first polyelectrolyte being deposited (*Decher 2003*). Measuring the zeta-potential is a way to study the changes in surface charge during the stepwise film assembly.

The main prerequisite for film formation is solvent accessible surfaces. However, tuning the multilayer build-up requires control of other parameters, such as salt concentration and pH. Other important parameters are polyelectrolyte concentration, temperature, adsorption time, solvent composition, density of charged groups, surface roughness, surrounding humidity, rinsing time, drying time, *etc* (*Decher 2003*).
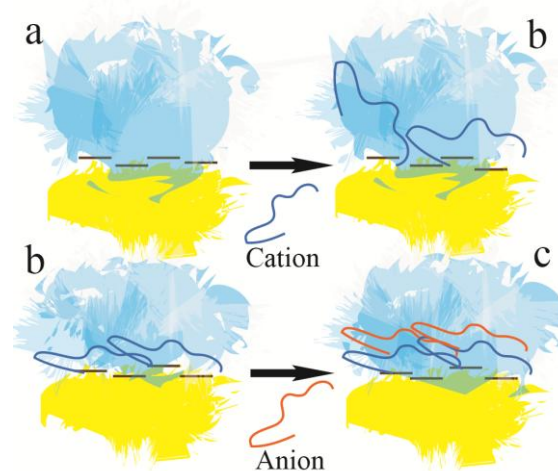
Figure 3.2 *Starting with a negatively charged surface immersed into a solution of (a) a cationic polyelectrolyte is deposited onto the surface, (b). After adsorption and reorganization an anionic polyelectrolyte is deposited onto the cationic surface, (c), and so on. A washing step between each polyelectrolyte deposition is required and numerous bilayers can be assembled.*

Reproducing the deposition conditions enables repeatable results which is especially important when handling weak polyelectrolytes, since they are far more sensitive to their surroundings than strong polyelectrolytes.

The thickness of assembled multilayers is directly dependent on the salt concentration, which is a straightforward way of controlling the thickness of the single layer, as well as the final film. The charge densities of the surface and of the

polyelectrolyte as well as the salt concentration affect the adsorption. Strong polyelectrolytes normally adsorb in small amounts when a low salt concentration is used, while increasing the salt concentrations leads to thicker layers, see Figure 3.3. However, the weaker and more sensitive polyelectrolytes have different adsorption patterns. A low ionic strength often promotes adsorption (*Fleer 1993*).

Having the pK_a of a weak polyelectrolyte in mind, it is possible to govern the conformational changes by altering the pH. Hence, a coil-like structure can be attained and the adsorption pattern will be similar to that for strong polyelectrolytes with a high ionic strength. Also, the type of polyions and the deposition conditions affect the film thickness, and as a general rule of thumb more layers are needed in a solution of low salt concentration to generate a multilayer as thick as that obtained at higher salt concentration. By changing the salt concentration in solution, the multilayer thickness can also be affected after assembly by rearranging the polyions through swelling or de-swelling. Film layers placed in a solution with high ionic strength often swells, and they de-swell if placed in a solution without salt. This behavior is influenced by the opening and closing of salt bridges between the oppositely charged polyelectrolyte layers and their counterions (*Decher 2003*). The first polyelectrolyte deposition will be strongly affected by the substrate charge and in order to facilitate the adsorption a primer such as PEI (polyethyleneimine) is sometimes used, promoting adsorption by creating a higher surface charge as the surface roughness is increased (*Decher 2003*).
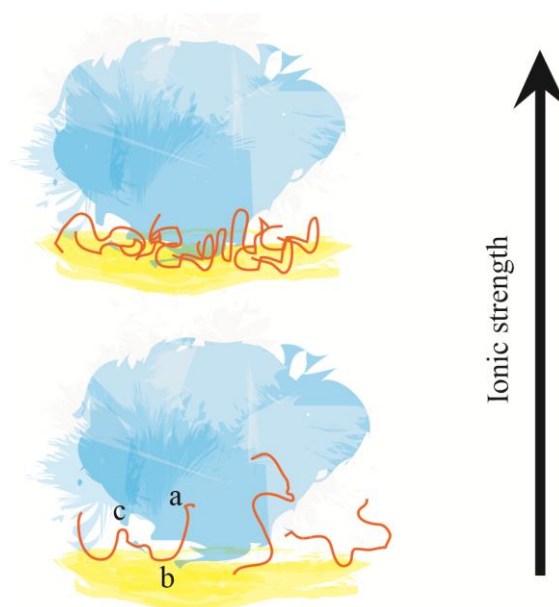
Figure 3.3 *Adsorption of strong cationic polyelectrolytes on a negatively charged substrate. Counterions and salt ions are not shown in this picture. With increasing ionic strength, the added ions contribute with a screening effect and the macromolecule forms a coil-like structure due to the decrease of the electrostatic repulsion between the monomer units. Hence the polyelectrolytes with lower salt concentration adsorb less and give a thinner and less dense film than the structure with higher ionic strength. The segments (a), (b) and (c) represent the tail, the train, and the loop, respectively.*

3.1.2 The Zone model

The zone model describes the multilayer structure in a simplified way during film formation, see Figure 3.4. Two areas are charged, Zones I and III, while Zone II is considered neutral. However, the actual multilayer film does not have such precise zones, as the polyelectrolytes constituting the structure intermingle, hence resulting in diffuse interfaces. Zone II is formed after Zones I and III, having forwarded an increasing charge from Area I to Area III. Consequently Zone II increases its thickness, while the two other zones remain constant as the multilayer grows. The polyelectrolyte molecules usually settle at the deposition site; nevertheless, each polymer chain intertwines with the

neighboring chain and creates a successive transition between the layers. The distribution of polymers in the middle of each plane, or the segment concentration profile, is determined by the spread of each individual polyelectrolyte as well as the average of different polyelectrolytes in one layer. The average layer thickness can simply be calculated by dividing the total film thickness with the number of deposited layers (*Decher 2003*). Polymer sequence and conditions during multi-layer assembly, especially salt concentration, dictates each unique layer formation. Being charge compensated, the second zone can be considered polyzwitterionic and should swell when in contact with a salt solution. The other two zones, particularly Zone III, will behave in an opposite way since they normally carry an excess charge, which means that they will swell in pure water. The surface potential is measured in the third Zone.
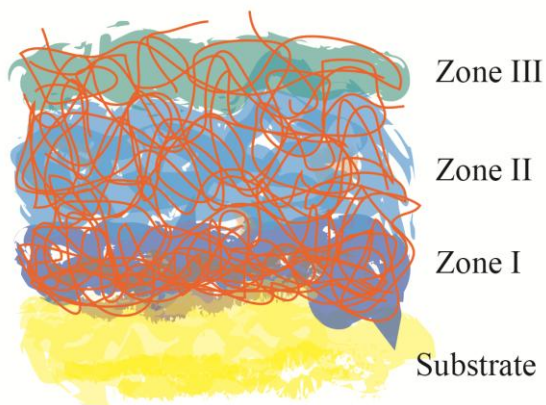

Figure 3.4 The zone model describes the multilayer film formation and structure in a simplified way. Zones I and III carry a net excess charge while Zone II is considered neutral. As the polyelectrolytes are deposited, Zone II is the only area that grows and the top and bottom areas stay at a constant thickness.

3.1.3 *Ex-situ* and *in-situ* studies of multilayer films

Multilayer films can be investigated either *ex-situ* or *in-situ*. An already assembled nanofilm can be studied with *e.g.* ellipsometry, AFM (atomic force microscopy) and NMR (nuclear magnetic resonance), while the process of assembling a film can be studied with *e.g.* QCM or QCM-D (quartz crystal microbalance without and with dissipation monitoring, respectively), *in-situ* spectroscopic ellipsometry and AFM (*in-situ* atomic force microscopy) (*Decher 2003*). QCM-D is a powerful tool for investigating adsorption kinetics for a variety of strong and weak polyelectrolytes and is described in detail in Chapter 4.2.

3.2 Polyelectrolyte nanofilms and biomedical applications

Cationic poly-L-lysine (PLL), poly allylamine hydrochloride (PAH) and anionic poly-L-glutamic acid (PLGA), hyaluronic acid (HA) are all weak polyelectrolytes that require strict control of pH during and after multilayer film assembly, but also polypeptide concentration, ionic strength, solvent composition and adsorption/rinsing time play a role. PLL, PLGA and HA are of interest for biomedical applications due to their biocompatibility and biodegradability (*Jessel 2003, Nitzan 2001*), and while PAH is biocompatible but not biodegradable (*Janeesh 2014*). For the application described in this thesis, uncontrolled release of incorporated actives can be avoided by creating a thin barrier of the mentioned polyelectrolytes. For instance, a stable PLL/PLGA film assembled under physiological conditions will be tightly

bound. Under such conditions the layers are tightly knit together mostly consisting of extended β-sheets (*Pilbat 2006*). The use of PLGA as the terminating layer ensures that the film surface facing the wound has a negative charge, which should minimize unwanted cell adhesion when in contact with a wound bed (*Richert 2004, Gergely 2004*). When studying the assembly of the PLL/PLGA nanofilm with both *in-situ* and *ex-situ* techniques, it has been shown that the multilayers normally have a water content of 60-70% (*Halthur 2004-I, Craig 2014*). PLL and PLGA polypeptides have previously been studied as coatings on implants for release of IL-12 (*Li 2009*) and release of cefazolin (*Li 2010*), for immobilizing proteins (*Halthur 2006*), and for tissue engineering matrices (*Hsieh 2005*). HA exists naturally in the body where it bears several functions (*Nitzan 2001*). Consequently, the polysaccharide has been widely used for biomedical applications. The company Bohus Biotech focusing on HA explains on their webpage that it can be used as cosmetic fillers, in facial creams, as a part of treatment of osteoarthritis (joint disease), and in drops or devices for ophthalmologic purposes. Research involving HA as component in thin films focuses on cell targeting and release of active substances (*Picart 2001, Szarpak 2010*). PAH is commercially available and hence used in many studies as a synthetic component in thin films, either as a component in a synthetic reference system to biodegradable thin films (*Marchenko 2012*) or in combination with a biodegradable component allowing it to rupture or swell for triggered release of actives (*Palamà 2011, Chung 2002, Wang 2008*).

3.3 Self-assembled monolayers on gold

Self-assembled monolayers (SAMs) are ordered structures that spontaneously form on a surface. For adsorption onto gold surfaces, alkane thiols are often used. The molecules have a terminal thiol group that readily adsorbs at gold from an ethanol solution, and the remaining part of the molecule can carry different functional groups depending on the application, see Figure 3.5. Sometimes monolayers are built up from a mixture of different alkane thiols. It has been reported that the ratio of two different alkane thiols in a monolayer at the surface need not to be the same as the ratio in solution (*Oskarsson 2006*). The composition of the monolayer reflects the relative solubilities of the alkane thiols in solution and the interactions between the tails. Also, alkane thiols are influenced by hydrogen bonding and other attractive interactions between polar end groups, which in turn affects the apparent hydrophilicity and, thus, the wettability (*Bain 1989-I*).

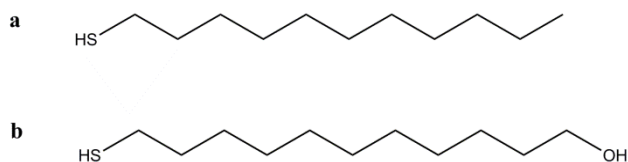***Figure 3.5*** *Structures of (a) 1-undecane thiol and (b) 11-hydroxy-1-undecane thiol.*

3.4 Active substances

When employing an active substance its mode of action needs to be considered. For antimicrobials the substance can have either a broad-spectrum or a more narrow-spectrum activity. This distinction is generally used for antibiotics; however, the antimicrobial effect of most antiseptics can

also be divided into a narrower or broader activity. For instance, the antiseptic effect of silver (Ag^+) is more pronounced on *Pseudomonas aeruginosa* than on *Staphylococcus aureus*, while for polyhexamethylene biguanide (PHMB) the antimicrobial effect is more pronounced on *S. aureus*. Quaternary ammonium compounds (QACs) are a popular group of antiseptics with varying antimicrobial effect. The cationic antiseptic is attracted to the negatively charged surfaces of a bacterial cell's membrane and can readily bind to its surface. The membrane usually has surrounding cations, *i.e.* Na^+, Mg^{2+} and Ca^{2+}, which are vital for the bacteria's osmoregulation. The Gram-negative bacteria's lipopolysaccharides and the Gram-positive bacteria's teichoic acid create their net negative charges (*Gilbert 2005*). The membranes' largest constituents are proteins with varying functions, *e.g.* structure or transport. The proteins can reach from the surface of the cell wall to the core of the cell, or be situated at a specific site on the surface of the cell membrane. The proteins are enclosed in a hydrophobic phospholipid bilayer with specific phospholipids as neighboring molecules to a specific protein.

Targeting the anionic bacterial cell membrane, many QACs are not very specific in their actions. Also, the QACs need to reach a particular chain length for optimal antimicrobial activity for both Gram-negative and Gram–positive bacteria (*Gilbert 2005*). The concentration of the active substance in QAC containing products is usually between 100-1000 times higher than the minimum inhibitory concentration (MIC), which is a contributing factor to why resistance does not seem to develop.

A cationic antimicrobial's most important feature is its charge, but it also needs a hydrophobic part, which can interact and disturb the phospholipid cell membrane. As a result, the interaction between the QAC and the membrane leads to leakage of counterions and consequently to disturbance of the osmoregulation in the cell. The holes may also lead to leakage of other intracellular components. The net result is that the cell dies. The quaternary ammonium compounds used in this thesis work are a betaine ester (tetradecyl betainate) and poly(hexamethylene biguanide).

Antibiotic substances are usually more specific in killing bacteria. For instance, the antibiotic used in this work, Vancomycin, inhibits the cell wall synthesis in Gram-positive bacteria, which eventually leads to bacterial death (*Rynolds 1989*). By having one single target, the bacteria can (and often will) adapt to the situation and develop resistance to a specific drug. Hence, it is of importance to control the administration of antibiotics and only use the drug when it is needed.

3.4.1 Betaine ester

Amphiphilic betaine esters, such as tetradecyl betainate, contain one hydrophilic and one hydrophobic moiety, where the betaine part originates from choline through natural metabolic oxidation. Hence, betaine contains a quaternary nitrogen in its structure. By esterification of betaine with a fatty alcohol, a betaine ester is formed. Betaine esters are extremely sensitive towards alkaline hydrolysis and they easily degrade when in contact with water with a pH slightly above neutral, generating betaine and a fatty alcohol, see Figure 3.6, both of which have low toxicity towards

mammalian cells. The reason for the very rapid alkaline hydrolysis of betaine esters is that the ester bond is unusually electrophilic and thus susceptible to attack by nucleophiles. The carbonyl carbon of the ester bond has a pronounced electron deficiency because of the electron-withdrawing effect of the adjacent quaternary ammonium group (*Thompson 1989*). The hydrolysis is strongly affected by pH and the degradation is faster at higher pH. For example, tetradecyl betainate (which is used in this thesis work) was hydrolyzed to 10 % at pH 6 after 18 hours, to 50 % at pH 7 after 8 hours, and to 90 % at pH 9 after 10 minutes (*Lindstedt 1990, Ahlström 1999-I*).

Binding of the betaine ester to the cell membrane is the first step of the bactericidal effect. However, if the pH is low, the bacterial membrane's net charge will decrease, which in turn results in less binding of the positively charged betaine ester to the membrane.
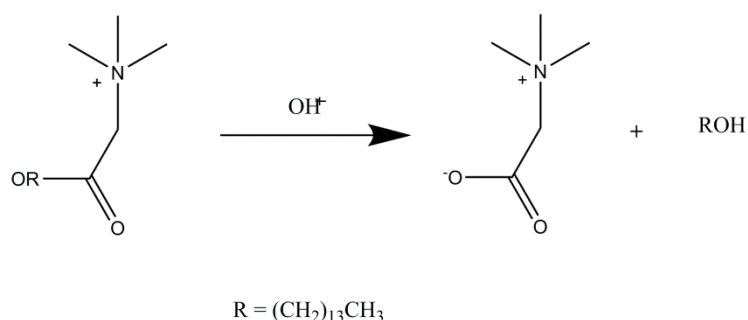

Figure 3.6 *Hydrolysis of betaine ester with a chain length of 14 carbons.*

The betaine ester's stability is also dependent on the temperature, with the rate of hydrolysis increasing with increasing temperature. The salt concentration also plays a role for the stability, with a decrease in hydrolysis rate with increasing salinity (*Lindstedt 1990*). The length of the alkyl chain determines the antimicrobial efficacy. Alkyl chains of the same length as that of the phospholipids in the cell membrane seem to have better killing effect than shorter ones. This would indicate that betaine esters of 16 and 18 carbons in the alkyl chain would be more efficient than the 14 carbon species used in this thesis work. However, the aqueous solubility of the betaine ester is also a parameter to consider. Long chain betaine esters are very insoluble in water and can therefore not be used in the concentration needed for sufficient antimicrobial effect (*Ahlström 1999-II, Ahlström 1999-III*). Considering both the strength of interaction with the membrane, which favors longer chain betaine esters, and solubility aspects, which favors shorter chain betaine esters, it seems that a betaine ester with 14 carbons in the hydrophobic tail is optimal for the purpose of this work.

3.4.2 Poly(hexamethylene biguanide)

Poly(hexamethylene biguanide) or PHMB is a bactericide used in swimming pools, contact lenses, cosmetics, cleanser in food handling, wound cleanser, as preservative of plasticized PVC, *etc* (*Gilbert 2005, Kaehn 2010*), see Figure 3.7. Being a quaternary ammonium compound, PHMB interacts with the negatively charged surface of bacterial cell membranes. PHMB has a broader antimicrobial spectrum than most other QACs. The MIC value for PHMB against *Staphylococcus aureus* is low compared to other QACs (about 1 mg/L), and so is its MIC against *Pseudomonas aeruginosa* (100 mg/liter) (*Paulus 2004*). Additionally, PHMB has low cytotoxicity; hence, at the working concentrations it seems not to affect human cells to the extent that other antiseptics often do (*Kramer 2004*). These two

properties, low MIC and low cytotoxicity, makes PHMB attractive for use as a single antimicrobial in a wound dressing. Similar to other QACs, PHMB's
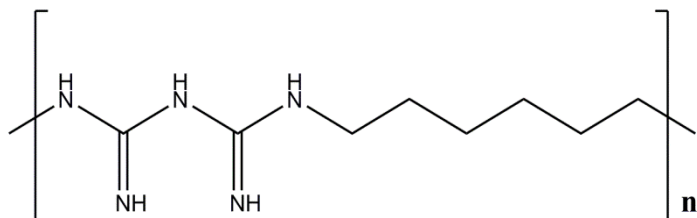

Figure 3.7 *Poly(hexamethylene biguanide) (PHMB). The best bactericidal effect is normally obtained with a value of n around 12.*

antimicrobial efficacy is dependent on the length of the alkyl chain. PHMB is an oligomer and it has been found that oligomers of more than ten repetitive units have a stronger antimicrobial efficacy than shorter ones (*Broxton 1983*). PHMB initially binds to single phospholipid sites on the bacterial cell membrane where maximum anionic charges are found. As the surrounding ions are dislodged from the cell surface, the attached antimicrobial polymers create clusters at the adsorption sites. Consequently, the PHMB domains transform the homogeneous phospholipid surface to a heterogeneous surface (*Broxton 1984-I, Broxton 1984-II, Broxton 1984-III, Ikeda 1984*). This transformation is detrimental to the cell wall functions, and leakage of surrounding cations is normally followed by leakage of increasingly larger molecules. As a conclusion, PHMB does not only have the same effective antimicrobial activity as other QACs, but by transforming the bacterial cell surface in a specific way makes it a very interesting biocide. As for resistance, PHMB does not show any evidence of resistance when used at appropriate concentrations (*Gilbert 2005*).

3.4.3 Vancomycin

Vancomycin is a glycopeptide antibiotic substance, which has been frequently used against Gram-positive bacterial infections for over fifty years (*Levine 2006*), see Figure 3.8.
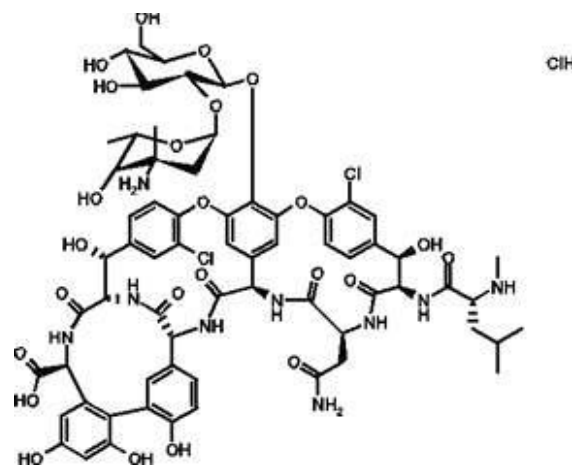
Figure 3.8 Vancomycin hydrochloride.

By inhibiting the cell wall peptidoglycan synthesis Vancomycin kills for instance *S. aureus* (*Reynolds 1989*), while Gram-negative species usually are left unaffected. However, Vancomycin anchored onto carriers has been shown to interact with P. aeruginosa cell membranes and enhance the antimicrobial action (*Kell 2008, Gu 2003, Gurunathan 2014*). The antibiotic substance is administered either as a solution (intravenously), orally or as a cream. Since Vancomycin has been used for decades, it is of little surprise that some Gram-positive species have developed drug resistance. Despite the resistance issues, Vancomycin is still used until new substances are cleared by the authorities. The use of Vancomycin in this project was as a model antibiotic, due to its solubility in water and the availability of fluorescent equivalents.

3.5 Wound infection and enzymes

Chronic wounds almost always have an underlying cause, *e.g.* diabetes. Consequently, poor blood circulation contributes to stalled healing together with other factors that disturb the normal wound healing cascade. Additionally, having an unfavorable environment for healing increases the risk for infection, allowing bacteria to contaminate, colonize and spread infection. All of the above conditions prevent the wound from healing, but the infection needs to be clinically addressed before any other treatment is considered.

Various bacteria normally colonize human skin, *e.g. Staphylococcus epidermidis*, *Corynebacteria*, *Staphylococcus aureus, etc*. The human microbiome benefits the host by for instance competing against pathogens and triggering the host immune system (*Todar 2012*). Consequently, when skin is compromised and a wound appears, bacteria of different types will also be present. A few of the bacteria in the normal human skin microbiome are pathogenic in deeper tissue and blood and can hence cause an infection. *Staphylococcus aureus* is an example of such a bacterium. Other pathogenic bacteria that normally do not exist on intact skin are also found in wounds and may cause difficult infections, for instance *Clostridium perfringes*, *Streptococcus pyregenes* and *Pseudomonas aeruginosa* (*Kirketorp-Møller 2011*). Three main stages portray the microbiology of the wound in a simplified way. Contamination is the first phase and relates to the fact that bacteria are only present in the wound. Colonization is the second stage, where bacteria present in the wound are multiplying; however, during

colonization no visual damage of the tissue is noticed. In some cases though, during the so called critical colonization stage, other unfavorable effects of wound healing can be seen. The third phase is infection, which is the stage when tissue damage by pathogens is clearly seen (*Edwards 2004*). The microbiological load on a chronic wound can be either superficial or found in deeper tissue, situations that obviously need different diagnostic tools, *i.e.* common swabs or biopsies. The swab can give information about shallow bacteria infecting a large area, while the biopsy gives information about bacteria embedded deeper into the wound tissue. There are both advantages and disadvantages with these techniques; however, the most commonly used and cheapest method for detection of infection today is the swab.

For protection against their host, many bacteria create a biofilm that hinders phagocytosis by human leucocytes (*Leid 2005*). Additionally, extracellular polysaccharides in biofilms also protect the colony of invaders as well as production of several different substances, such as toxins and proteases, which weakens the host's response to the infection (*Vuong 2004, Greener 2005, Jensen 2010*). Chronic wounds exhibit increased levels of proinflammatory cytokines and matrix metalloproteinases (MMPs), which seem to be produced in response to biofilm content, *i.e.* polysaccharides, peptidoglycans, *etc*. Bjarnsholt *et al*. describes the properties of a chronic wound as dependent on the proximity of the bacterial biofilm (*Bjarnsholt 2007*), while biofilms are less common in acute wounds. Systemic antibiotics have often had far less success in treating bacteria in biofilm than as free specimens, and may be up to 1000 times less effective. Biofilms may therefore

promote development of resistance. However, local treatment with some antimicrobial substances is more effective at penetrating biofilms and killing bacteria (*Alandejani 2009, Daeschlein 2013, Brackman 2013*), particularly in combination with wound debridement (*Wolcott 2010*). This supports the concept of a "smart" drug delivery material that releases an active substance if the wound shows signs of infection.

The chronic wound environment contributes to an increase in pH compared to an acute wound, *i.e.* the pH ends up around 7-8, which is favorable for the activity of many of the bacteria's proteases (*Dissemond 2003*). In some cases the pH well exceeds 8. Hence, the amount of bacterial proteases is high in infected chronic wounds (*Bowler 1998, Landis 2008*) and contributes to delayed healing. The proteases are exuded as a smokescreen to dim the presence of bacteria from the human immune system, which is done by degrading cytokines, antibodies, antimicrobial peptides, host tissue, *etc*.

3.5.1 *Staphylococcus auerus and glutamyl endopeptidase*

Staphylococcus aureus is a bacterium present on normal skin flora. As a consequence, the bacteria can contaminate broken skin if a lesion or wound is present. The bacterium is normally not a problem; however, if the patient has an underlying cause for delayed healing or if some strains such as MRSA (meticillin resistant *Stapylococcus aureus*) contaminate the wound, severe infections may occur. The bacterium is Gram-positive and belongs to the facultatively anaerobic family of *Staphylococcaceae*. *S. aureus* is shaped as spheres with a diameter of approximately 1

μm and forms clusters as it grows (*Todar 2012*). As a mechanism to stay unnoticed by the human immune system, the bacteria excrete several virulence factors, *e.g.* toxins and enzymes. Other exoproteases, such as glutamyl endopeptidase, or V8, contributes indirectly to virulence. By exuding V8, host tissue is degraded into low molecular weight molecules, which act as nutrients for the bacterium. As the bacteria grow stronger and multiply with the help of proteolytic enzymes, V8 also inactivates bacterial host responses, thus also facilitating bacterial colonization and infection (*Honeyman 2002*). Since chronic wounds have an elevated pH and since the activity of the enzyme is at its peak at pH 8, the wound environment is highly favorable for V8 proteases.

Glutamyl endopeptidase is an extracellular endopeptidase, which means that it cleaves bonds within a molecule, in this case peptide bonds solely on the carbonyl side of glutamate (Glu) and aspartate (Asp) residues. The cleavage next to Glu is 1000 fold faster than that next to Asp (*Sorensen 1991*). Due to the protease's specificity it is used for selective cleavage of proteins for peptide mapping. It belongs to the family of glutamyl endopeptidase I and is a serine protease. However, V8, with its 336 amino acids, has few analogs and it has only slight sequence identity with other serine proteases. For instance, the sequence identity with bovine trypsin is only 13 % and with its homologue glutamyl endopeptidase from *Staphylococcus epidermidis* 59 % (*Ohara-Nemoto 2002, Prasad 2004, Nemoto 2008*). It is also found that its specificity depends on the N-terminus, which is very uncommon among proteases. V8 carries a net negative charge; however, the positively charged N-terminus seems to have a large impact on

the enzyme's activity (*Prasad 2004, Ono 2010*). Certain buffers can inhibit the enzyme; however, it does not affect the protease's specificity (*Sorensen 1991*). All properties of V8 contribute to its success to impair host tissue and inactivate host responses. Its substrate specificity is taken advantage of in this thesis work for designing a release system for antimicrobials.

3.5.2 *Pseudomonas aeruginosa* and Protease IV

Pseudomonas aeruginosa is a Gram-negative bacterium with opportunistic tendencies. Hosts with compromised health are hence more vulnerable against the pathogenic strains causing infection at several (host) sites, *e.g.* in soft tissue, bone, cartilage, lungs, *etc*. However, *P. aeruginosa* is foremost a nosocomial pathogen (*Todar 2012*). The bacterium has a rod-like structure and belongs to the family of Pseudomonadacea, which often is found in soil and water. Like *S. aureus*, aerobic *P. aeruginosa* possesses facultative behavior, and is even called a facultative anaerobe by some, due to its ability to survive in environments with little or no oxygen. Generally, the use of oxygen is exchanged for the use of NO_3, enabling it to multiply despite harsh surroundings. This fascinating bacterium is famous for moving exceptionally fast, its ability to grow even in distilled water, being tolerant to many antimicrobial substances, to high or low temperatures and biofilm formation. Similar to *S. aureus, P. aeruginosa* exudes many different chemicals as protection. We have focused on the protease called Protease IV, which can be expressed in *Escherichia coli* and is then called rLysC. The protease is characteristic for the *P. aeruginosa* bacterium and no other bacteria in the same or other families carry the Protease IV gene. Whether or not, or to what extent, most other virulence factors are exuded vary on strain and depends on

the surroundings; however, protease IV seems to be the one virulence factor that always is exuded (*Caballero 2004*). In other words Protease IV is a very important virulence factor for *Pseudomonas aeruginosa*. The serine protease is lysine-specific and attacks the carboxyl side of lysine bonds in peptides. The action leads to tissue damage and also strengthens the bacterium's stronghold by degrading host immunoresponse molecules (*Engel 1998, Wilderman 2001*).

3.5.3 Human neutrophil elastase

Human neutrophil elastase (HNE) is a serine protease commonly found in wounds. HNE exists in azurophil granules in neutrophils, which are successful phagocytes that constitute a major part of host defense when faced with an infection (*Pham 2006*). HNE has a wide spectrum of target substrates and degrades collagen, elastin and proteoglycans in the extracellular matrix, as well as the outer membrane of some bacteria, fungi and certain virulence factors. In other words, together with HNE inhibitors, this elastase participates in the wound healing process. However, with a deficiency in inhibitor molecules, the tissue will be degraded in an uncontrollable manner, which is the case with many diseases striking the pulmonary airways (*Pham 2006*). 218 amino acids form the chymotrypsin-resembling neutrophil elastase with a net positive charge and the enzyme prefers hydrophobic substrates (*Sinha 1987, Siedle 2007*). Since HNE has a broad spectrum of substrate specificity and is commonly found in wounds, it was decided to use this enzyme for studies of degradation of the polypeptide film in a noninfectious environment.

3.5.4 Trypsin

Bovine trypsin is a serine protease that cleaves a protein at the C-terminal of lysine (Lys) and arginine (Arg), but only when the preferred amino acid does not bind to proline (Pro). Trypsin is specific for positively charged substrates (*Schrøder-Leiros 2004*). Being a serine protease with some similarity to glutamyl endopeptidase (V8) (*Prasad 2004*), trypsin was chosen as reference enzyme in the 2D nanofilm degradation studies.

4 ANALYTICAL TECHNIQUES

4.1 Contact angle

Contact angle measurements are widely used in research and for quality control of surfaces. Wetting of surfaces is related to the interfacial tensions between solid, gas and liquid, which is described by Young's equation in Equation [1]:

$$\sigma_{SV} - \sigma_{SL} = \sigma_{LV} \cos \theta_Y \qquad [1]$$

where σ_{SV}, σ_{SL} and σ_{LV} are the interfacial tensions between solid-vapor, solid-liquid and liquid-vapor, respectively. A system with water as the liquid phase is described in Figure 4.1. If the substrate is hydrophobic, then $\theta > 90^o$, since the droplet does not wet the surface. On a hydrophilic substrate ($\theta < 90^o$), on the other hand, the droplet partially or fully wets the surface.
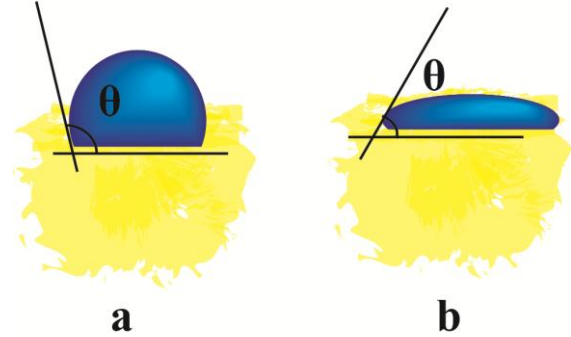

Figure 4.1 *A drop of water on (a) a hydrophobic surface and (b) a hydrophilic surface. θ describes the angle of the droplet, which if larger than 90° indicates a hydrophobic surface, and if less than 90°, a hydrophilic surface, based on the ability of the droplet to wet the surface.*

4.2 Quartz crystal microbalance with dissipation monitoring

Quartz crystal microbalance with dissipation monitoring (QCM-D) is a powerful technique for studies of adsorption and desorption kinetics on surfaces. The technique has been thoroughly presented in the literature (*Rodahl 1996, Höök 1998*). There is considerable interest in the use of the technique within the biochemical area (*Höök 2007*).

Sauerbrey reported in 1959 that the mass of molecules deposited on a QCM sensor can be measured by studying the decrease in frequency (*Sauerbrey 1959*). The frequency and the mass are proportional as long as they fulfill three requirements: the deposited mass must be substantially smaller than the weight of the crystal, the molecules must be firmly adsorbed, and the adsorbed mass must be evenly distributed. Provided that these requirements are fulfilled the adsorbed (or desorbed) mass, Δm, changes the oscillation frequency, Δf, of the sensor crystal, as described by the Sauerbrey equation [2].

$$\Delta m = \frac{\Delta f \times C}{n} \qquad [2]$$

In Equation [2], C is the mass sensitivity constant, 17.7 ng Hz^{-1} cm^{-2} for a quartz sensor with $f = 5\,MHz$, and n is the overtone number (n = 1, 3, 5, 7, …), and it assumes that the loss of energy of oscillation through the film is negligible (*Vogt 2004*). The thickness of the adsorbed layer can be estimated using Equation [3], where ρ_{eff} is the adsorbed layers' effective density.

$$d_{eff} = \frac{\Delta m}{\rho_{eff}} \qquad [3]$$

The substrate used in QCM is a piezoelectric quartz sensor crystal, which oscillates at its own frequency when applied to an electric field. Later studies have revealed that for frequency and mass to be proportional to variable films properties with inevitable variations in hydration and hence the damping of the deposited matter, the driving voltage should be periodically shut off (*Rodahl 1996*). By switching off the power it is possible to study how the oscillation decays exponentially with time (see Figure 4.2), therefore also including the viscoelasticity of a film when calculating Δm, which otherwise would be underestimated if using Equation [2] (*Höök 2001-I*). The time of decay, τ, can be translated into the dissipation factor, ΔD, by measuring the subsequent amplitude signal, $A(t)$ (*Rodahl 1996, Voinova 1999*). The amplitude is then fitted numerically, which in turn gives the equation shown in [4], describing ΔD for the dissipated energy during a single dissipation (*Rodahl 1995, Rodahl 1996*),

$$\Delta D = \frac{1}{\pi f \tau} = \frac{E_{dissipation}}{2\pi E_{stored}} \qquad [4]$$

where $E_{dissipation}$ stands for loss in energy and E_{stored} is the stored energy of the adsorbed layer. For a viscoelastic fluid, the Maxwell viscoelastic model is normally used when calculating mass (or viscosity) for the adsorbed matter. For a viscoelastic solid, the Voigt (Voigt-Kelvin) model is used (*Voinova 1999*), see Figure 4.3. Viscoelastic films, *e.g.* adsorbed polymers, have a higher dissipation and require a more complex mathematical model for simulation of the adsorbed mass, *e.g.* the

Voigt based viscoelastic film model. The Voigt model describes propagation and damping of acoustic waves in a single undifferentiated viscoelastic adsorbed film in contact with a Newtonian bulk liquid (*Voinova 1999, Höök 2001-II*).

Adsorbed layers that have frequency dependent viscoelastic properties express a shear modulus, G^*, which is related to the storage modulus, G', and the loss modulus, G''. These parameters can in turn be related to the elastic shear (elasticity) of the film and the film's viscosity, respectively (*Cho 2007*).
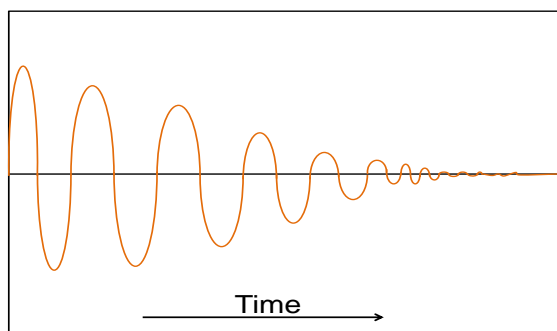
for viscoelastic films the mathematical dependence of Δf and ΔD and the film's mechanical properties have been further refined by Voinova *et al* (*Voinova 1999*). The parameters concerning the quartz crystal and the solvent (bulk) are in most cases known, but the film parameters need to fit the viscoelastic model of choice after approximating the film density.

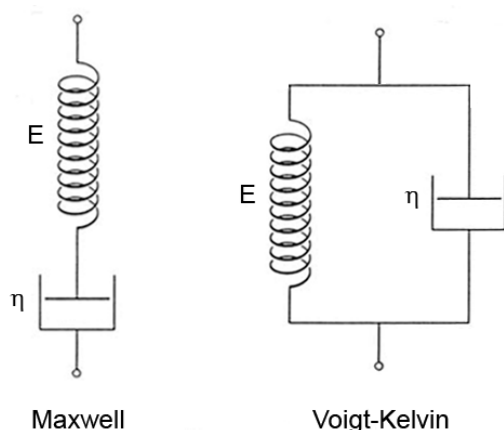**Fig. 4.2** *Oscillation decaying with time as the driving voltage is shut off.*

Maxwell   Voigt-Kelvin

Figure 4.3 *The Maxwell and Voigt viscoelastic models include a spring with E as the elastic modulus and a dashpot with η as the viscosity. The spring describes the applied stress, σ, according to Hooke's law, and the stress for the dashpot is expressed by Newton's law, $\sigma = E \cdot \gamma$ and $\sigma = \eta \frac{d\gamma}{dt}$, where γ is the strain. As for the Maxwell element, it has a uniform distribution of stress, $\sigma = \sigma_{spring} = \sigma_{dashpot}$, while the Voigt element has a uniform distribution of strain, $\gamma = \gamma_{spring} = \gamma_{dashpot}$. Consequently, the Maxwell element's strain and the Voigt element's stress are both assumed to be additive and expressed as $\gamma = \gamma_{spring} + \gamma_{dashpot}$ and $\sigma = \sigma_{spring} + \sigma_{dashpot}$, respectively.*

As can be seen in Figure 4.4, the frequency and the dissipation are dependent on a number of film properties. For rigid films the Sauerbrey relation is valid; however,
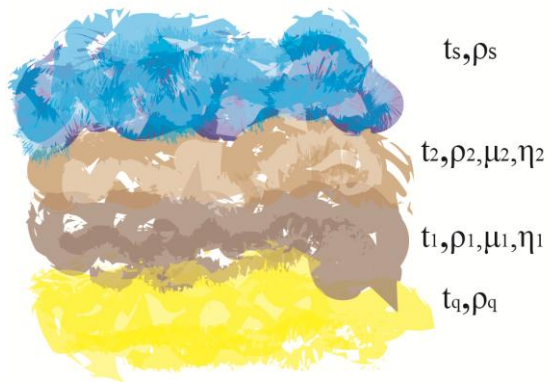
Figure 4.4 *Parameters involved in calculating Δf and ΔD for a viscolelastic film. As in the literature (Voinova 1999), this example describes a film with two layers on top of a quartz crystal, q, in a Newtonian bulk solvent, s, where the parameters are used in a Voigt based model.t is the thickness, ρ the density, μ the elastic shear modulus (or G') and η the viscosity. However, the viscous penetration depth, δ, is also a necessary parameter.*

4.3 Ellipsometry

Ellipsometry is an optical technique used for studies of the dielectric properties of thin films, and it has been thoroughly described in the literature (*Azzam 1987, Tompkins 2005*). In brief, the change of polarization of light reflected (or transmitted) off a sample gives information about the thin film, see Figure 4.5. A specific sample's known parameters often decide which and how much information the ellipsometry measurements can give. In two situations a direct inversion of the ellipsometric angles, Ψ and ρ, can be performed for retrieving the optical constants of a studied substrate. The first situation is when the only unknowns are the optical constants for a substrate and the second situation is when all is known except the thickness (*Azzam 1987*). However, more often, a mathematical model is used to iteratively reach the optical constants from the output (ellipsometric angles). The latter is done with advanced software, where information is available for interpretation and modeling of data, *e.g.* calculation of film thickness. When studying the thickness of a film, the angle of incidence is decided after measurements along the normal of the sample. A sweep over a range of wavelengths is also performed to find the wavelength suitable for the specific substrate. For studies of the sample's anisotropy, the substrates are rotated and measured again.
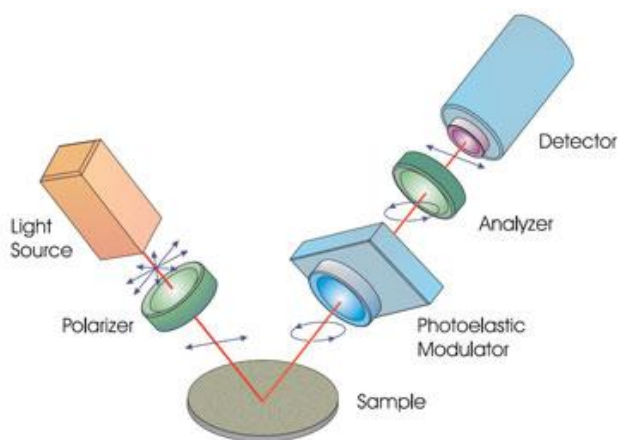

Figure 4.5 *Schematic description of spectroscopic ellipsometry. (www.azom.com)*

5 EXPERIMENTAL METHODS

For specific concentrations and other details, please see the Papers in the end of this work.

5.1 Polyelectrolyte solutions, enzyme solutions and crosslinking

5.1.1 Preparation of polyelectrolyte solutions

The polyelectrolytes used were poly-L-lysine hydrobromide (PLL) ($MW = 84\ kDa$), poly-L-glutamic acid sodium chloride (PLGA) ($MW = 120\ kDa$), polyallylamine hydrochloride (PAH) ($MW = 900\ kDa$) and hyaluronic acid (HA) ($MW = 2.5 - 2.7\ MDa$). A Tris-HCl buffer solution was prepared with NaCl (0.1 M for 2D film and 0.15 M for the spheres and capsules). For 2D films and the films on the o/w emulsion spheres, PLL and PLGA were added in an amount corresponding to 1 mg ml⁻¹. For 3D films on template assisted assembly microspheres, PLL, PLGA and PAH were added at 4 mg ml⁻¹, and HA at 5 mg ml⁻¹. The LbL assembly was prepared at pH 7.4.

5.1.2 Preparation of enzyme solutions

The bacterial proteases used were V8 proteinase or glutamyl endopeptidase originating from *Staphylococcus aureus*, and Protease IV, originating from *Pseudomonas aeruginosa* (expressed in *E. coli*, then called rLys-C) Reference enzymes were human neutrophil elastase (HNE) and trypsin (bovine pancreas). V8 and Protease IV were diluted to concentrations related to an amount related to concentrations found in infected wounds (*Prof. M.D. Artur Schmidtchen, personal communication*). HNE enzyme solutions were diluted to 1:100 or 1:8. Trypsin was used at different concentrations ranging from 1 wt% (1:100) to equal amounts of each (1:1 weight ratio solution). Trypsin was only used on the 2D nanofilm.

5.2 Polyelectrolyte nanofilms – *2D*

5.2.1 Gold surfaces and characterization of nonwoven and tailoring of gold sensor surfaces

The QCM-D sensors were cleaned in an UV/Ozone (UVO) chamber combined with a treatment using an ammonia-hydrogen peroxide mixture. If the sensors were not used immediately, they were stored for maximum 7 days in ethanol. The nonwoven of choice was hydrophilic (θ < 90°) and viscose based, thus cellophane was used as a non-absorbing reference material. Contact angle measurements were used to study the materials' wetting. The tailored gold sensor surface was achieved combining 11-hydroxy-1-undecanethiol with 1-undecanethiol.

5.2.2 QCM-D: assembly of and enzymatic exposure to nanofilms

Tailored gold sensors were either placed in a QCM-D D-300 or a QCM-D E4 for measurements during LbL assembly and during degradation studies. A stable signal ($\Delta f, \Delta D$) was achieved before adding either a new polyelectrolyte or buffer solution. The stepwise procedure was repeated until three bilayers, (PLL/PLGA)₃, were formed on the SAM coated surface. The sensors were either

kept wet in the chamber or dried before an enzyme was added for studies of enzymatic exposure. Analysis of film assembly and thickness was performed in Q-Tools.

5.2.3 Ellipsometry

Ellipsometry measurements were performed at ambient temperature using wavelengths between 196-2000 nm. The ellipsometer operates with an elasto-optic modulator. TFCompanion software was used for the data analysis. The measurements in UV light with a deuterium lamp did not give a good fit for the current system; however, data analysis showed a good fit in visible light between 400 to 799 nm with the monochromator locked at 633 nm. The dual measurements were done to avoid possible disturbances from the reflective gold surface. The angle of incidence was set to 60°. The ellipsometry samples can be seen in Table 5.1. Each sample was rotated 90° and then 180° to study possible sample anisotropy. Additional measurements were performed when the gold substrates had been plasma treated, due to an increased surface roughness.

Sample	Modification / Film assembly
1	Au
2	Au-SAM
3	(Au-SAM)-(PLL/PLGA)
4	(Au-SAM)-(PLL/PLGA)$_2$
5	(Au-SAM)-(PLL/PLGA)$_3$

Table 5.1 *Samples used in the ellipsometry measurements.*

5.3 Polyelectrolyte nanofilms – 3D

5.3.1 o/w emulsion assembly of microspheres

The o/w emulsion was made by using a high shear homogenizer and PLGA as emulsifier. The oil phase was either glyceryl trioctanoate (GTO) or a 1:1 ratio mix of GTO and corn oil. The pure GTO contained 0.1-1 wt% betaine ester, and the oil mix contained 0.01 wt% Nile Red. The emulsion was washed three times by centrifugation at 10 000 rpm for 1 h. The emulsion was added dropwise to a solution of a polypeptide of opposite charge to the previous layer for LbL adsorption and nanofilm build-up. Centrifugation and LbL adsorption were repeated until 3 or 5 layers were assembled.

5.3.2 Template assisted assembly of microcapsules with PAH/PLGA shells

$CaCO_3$ spheres were used as sacrificial templates. The porous calcium carbonate microspheres had an average size of 3 μm (range: 0-10 μm). The spheres were suspended at a concentration of 2 wt% before ultrasonication. The large polycation, PAH, was added before washing the solution by centrigugation three times (3 500 rpm for 5 min) and then the anionic PLGA was added. The LbL procedure was repeated until 6 layers were created, *i.e.* (PAH/PLGA)$_3$. The next step was to crosslink the nanofilm, see Chapter 5.3.4. After stabilization of the PAH/PLGA shell, a 4 % gluconolactone solution with 0.02M MES buffer (see Chapter 5.3.4) was added to the capsule suspension to carefully dissolve the $CaCO_3$ templates. The capsules were kept in suspension and under stirring. In all steps, the ζ-potential was measured.

5.3.3 Template assisted assembly of microcapsules with HA/PLL shells

(HA/PLL)$_3$ nanofilm shells were prepared in the same way as the (PAH/PLL)$_3$ shells, see Chapter 5.3.2. The only differences was that anionic polyelectrolyte was added first, HA had a concentration of 5 mg/ml, and the centrifugation speed during washing needed to be increased to approximately 4000 rpm when HA was the added layer.

5.3.4 Crosslinking the films

To stabilize the films assembled in Chapters 5.3.1 to 5.3.3, peptide bonds were created by crosslinking. Before crosslinking the nanofilms the buffer was changed to 2-(N-morpholino)ethanesulfonic acid sodium salt (MES) including NaCl. Crosslinking agents were N-(3-dimethylaminopropyl)-N'-ethylcarbodiim-ide hydrochloride (EDC) and N-hydroxysulfosuccinimide sodium salt (sulfo-NHS). The concentration of EDC was varied between 25 mM to 200 mM, and the concentration of sulfo-NHS between 25 to 50 mM. The final washing step was performed with centrifugation or dialysis while stirring.

5.3.5 Loading of microcapsules

Loading was initially performed by adding suspended capsules to a probe or drug solution (ratio 1:1). A FITC-dextran ($MW = 4\ kDa$) in MES buffer was used as the main model drug. The ionic strength was varied between 0.15, 0.5, 0.75 and 1.25 M. Additional tests were performed with other fluorescent model drugs with better resemblance to the actual drugs, *i.e.* Rhodamine green ($MW = 3\ kDa$, cationic)

comparable to PHMB ($MW \approx 2.7\ kDa$) and Vancomycin BODIPY ($MW \approx 1.7\ kDa$, neutral at pH 7) comparable to Vancomycin ($MW = 1.4\ kDa$). All loaded microcapsules with fluorescent probes were investigated in a fluorescence microscope with x63 optical zoom. The loading of the actual drugs were performed in the same way. Removal of excess drug was done by either filtration or dialysis (while stirring). Also, the loading capacity was investigated by studying the remaining drug in the surrounding solution. The loaded microcapsules were separated from the solution using a hydrophilic syringe filter, and the surrounding liquid was studied in NMR.

5.3.6 Light microscopy

Samples were continuously studied in a light microscope, where the capsule size and their cumulative distribution were investigated.

5.3.7 Zetasizer

The surface charge of all microspheres and microcapsules were studied after each added polyelectrolyte layer (after wash by centrifugation) using a Malvern Zetasizer Nano Range.

5.3.8 Environmental SEM

Environmental scanning electron microscopy (ESEM) was initially used to study crosslinked microcapsules and spheres The ESEM can be used in both high and low vacuum mode, as well as in the ESEM mode. However, the resolution was considered to be too poor for further use. Only a few images were received after the water had been vaporized at 4.93 Torr (657 Pa) and 1 ^{o}C (5 kV electron beam).

5.3.9 SEM

Samples were either air dried or freeze dried on scanning electron microscope (SEM) holders. The freeze drying was performed at -110 ^{o}C. All samples were sputtered with gold in a 2 x 30 seconds cycle.

5.3.10 Confocal laser scanning microscopy

Microspheres were studied after crosslinking in a confocal laser scanning microscope (CLSM) using a Plan APO 20x magnification 0.7 NA dry air objective lens, when the microcapsules or spheres had been loaded with a probe.

5.3.11 NMR

Quantitative ^{1}H NMR spectra were acquired using a 400 MHz spectrometer. Prepared samples contained 10 % D_2O to allow for a sufficient lock signal. Complementary self-diffusion experiments were recorded using a 600 MHz spectrometer. All NMR experiments in this work were carried out at 25 °C. For the spectral analysis and integral calculations, the software program MestReNova version 8.1.2 was used. The loading capacity and the spectral determination of PHMB concentration was established by integration of the NMR signals corresponding to the aliphatic hydrogens. An aqueous stock solution of 3 wt% PHMB was used a reference. Spectral determination of Vancomycin concentration was established by integration of the NMR signals corresponding to the methyl hydrogens. An aqueous stock solution of 1 mM Vancomycin was used a reference.

5.3.12 Enzymatic degradation

The crosslinked and enzymatically ruptured microcapsules loaded with 4kD FITC-dextran were studied in a CLSM with objective HCX PL APO CS WATER UV with 63 times magnification and a numerical aperture of 1.20 with optical zoom ×4, ×6.5 and ×20. FITC-dextran was excited by a 488 nm argon laser and the emitted signal was recorded in the wavelength interval 510-550 nm.

5.3.13 Antimicrobial efficacy

The pathogenic bacterial strains used for efficacy studies of HA/PLL microcapsules was ATCC 29260 (*Pseudomonas aeruginosa*, PA 103) and for the PAH/PLGA microcapsules ATCC 49775 (*Staphylococcus aureus*, strain V8). The freeze dried strains were placed in an overnight culture of tryptic soy broth before dilution in simulated wound fluid (SWF) consisting of calf serum and peptone water in a ratio of 1:1. The working bacterial dilution of 10^6 cells/mL was achieved after adding the microcapsule suspension (1:1 ratio) in a 6-well cell culture plate, thus resulting in a final concentration of about 1.5 vol% microcapsule suspension. Suspensions were mixed and then placed in an incubator at 35 ± 2 ^{o}C and 200 rpm. Sampling was performed after mixing the suspension with a pipette at 3 and at 24 hours by adding 0.1 mL of sample to 0.9 mL of peptone water. The same procedure was repeated for the reference (hollow and empty microcapsule suspension) and the control (bacteria only). Each sample were made in three replicates.

6 RESULTS AND DISCUSSION

6.1 Characterization of nonwoven and tailoring of gold sensor surfaces

Nonwoven is used in wound care either as an absorbing material in direct contact with the wound or as the core of a complex dressing. The sterilized, viscose based nonwoven was found to be hydrophilic compared to standard nonwoven webs made of *e.g.* polypropylene. Since the nonwoven material is absorbing, cellophane was used as reference during the contact angle measurements. Cellophane and nonwoven are both regenerated cellulose products and were expected to have a similar surface chemistry with hydroxyl and methylene groups dominating the surface. This was also confirmed since the contact angle received was 70 ± 2° for both materials. To tailor a surface that imitated nonwoven, an alkane thiol with a terminal hydroxyl group and one with a terminal methyl group were mixed in varying ratios in ethanol and assembled on QCM gold sensors. The ratio of alkane thiols in solution and in a self-assembled monolayer, SAM, need not be the same (*Bain 1989-I*) since the composition reflects the relative solubilities of the alkane thiols in solution and the interactions between the tails. A 60 to 40 molar ratio of hydroxyl to methyl terminated alkane thiol resulted in a contact angle of 72 ± 1°, which is in accordance with previously reported values (*Oskarsson 2006*). Hence, this composition was chosen when creating the model surface for the QCM-D and ellipsometry

measurements. Contact angle results obtained for the SAM surfaces were repeatable and did not vary with time, indicating that the C11 alkane thiol chains were long enough to give a stable monolayer. It has been claimed that longer chains, C16-C24, create more stable layers (*Everhart 2002*); however, it seemed to be sufficient with C11 chains in this study. Furthermore, PLL/PLGA multilayers built on C11 thiols resulted in a repeatable layer thickness, whereas the layers built on C16 thiols had greater variation in thickness. The alkane thiols of choice are presented in Figure 3.5.

6.2 PLL/PLGA *2D* nanofilm assembly on nonwoven, cellophane and tailored gold surfaces

6.2.1 Film assembly

The PLL/PLGA nanofilm was deposited onto the hydrophilic nonwoven material to investigate the change in contact angle. Also, a non-absorbing cellophane sheet was used as the reference substrate. Both substrates had an initial contact angle of approximately 70°. The absorbing nonwoven was just manageable in the previous contact angle measurements, but after the crude process of dipping and drying, the wetting of the material was too fast to be measured. However, the contact angle of the treated cellophane substrate decreased from 70° to 35°. The nanofilm was then deposited onto the SAM treated gold substrates, which resulted in a slightly lower contact angle, approximately 30°.

6.2.2 PLL/PLGA nanofilm assembly studied with QCM-D

QCM-D is a gravimetric measurement technique, which in this work measures the amount of adsorbed polyelectrolytes as well as the incorporated solvent *in-situ*. A stable baseline was obtained after the buffer injection and after allowing the temperature to stabilize at 22.5 $^{\circ}$C. Adsorption of polyelectrolytes on the SAM covered gold sensors was monitored at the third, fifth and seventh overtone, and the variation of frequency was normalized versus the overtone. As Figure 6.1 describes, the cationic PLL adsorbed readily to the negatively charged alkane thiol surface, hence forming a stable foundation for the subsequent layer-by-layer assembly. The frequency decrease in Figure 6.1 indicates an increase in mass. Weak polyelectrolytes have a high degree of motional freedom, which should be observed by an increase in dissipation. However, the rapid adsorption of the first bilayer only gave small shifts in both frequency and dissipation. Such an event suggests limited possibilities for rearrangements. The measurements on the second and third bilayers indicated adsorption in loops and tails as well as possible penetration into underlying layers, as expressed by larger frequency shifts. As expected, the dissipation increased for the subsequent layers, indicating a three-dimensional film structure with solvent trapped in the film cavities. It was important to have control of the so-called bulk effect, *i.e.* the effect of the viscosity and the density of the surrounding liquid on the multilayer response, see Figure 4.4. Hence, the samples were rinsed after each polyelectrolyte addition to minimize the effect of the bulk. Together with the fact

that a low polypeptide concentration was used during assembly, the bulk effect was considered to be small enough to be ignored (*Knag 2004, Bordes 2010*). Also, viscosity measurements showed little difference between the polyelectrolyte solutions and water.
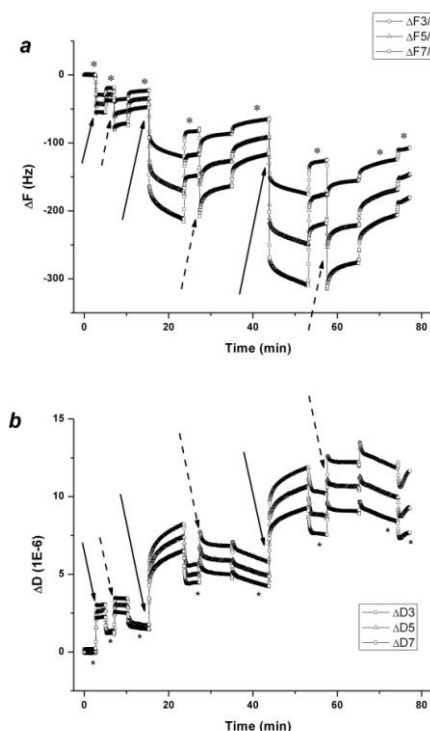

Figure 6.1 *QCM-D measurements describing the shift in frequency in (a) and the dissipation in (b). As seen in both graphs, three PLL/PLGA bilayers are assembled with buffer rinsing steps (*) between each polypeptide addition as a means to minimize the bulk effect. Full arrows indicate addition of PLL and dashed arrows indicate addition of PLGA.*

The viscoelastic character of the film is expressed by the lack of overlap in the frequency response while $\Delta D > 0$. For evaluation of the QCM-D results, a viscoelastic Voigt-based model was used in Q-Tools, see Figure 4.3 (*Voinova 1999*). This particular model is usually a good

representation for near to solid polyelectrolyte multilayer films and is well documented in the literature (*Voinova 1999, Voinova 2002*). By assuming a known density, the relationship in Equation 5 was utilized.

$$thickness = \frac{mass\ per\ surface\ area}{density} \qquad [5]$$

The mass per surface area is expressed in $kg \cdot m^{-2}$, the thickness in m, and the density in $kg \cdot m^{-3}$. For the polypeptide film layers, a density of $1200\ kg \cdot m^{-3}$ was used (*Höök 2001-II, Höök 2002*). The data from Figure 6.1 fitted well for the third, fifth and seventh overtones, and Equation 5 was used to obtain the gradual build-up of mass during film assembly in Figure 6.2. The total thickness of three PLL/PLGA bilayers ended up at $10 \pm 1\ nm$. Figure 6.2 shows the rapid formation of the first bilayer and that steady state is quickly reached. However, polypeptide films are often referred to as "soft", which is clearly observed in the subsequent bilayers. These layers take longer to reach steady state due to polymer reorganization after a fast initial adsorption. This behavior normally occurs after the formation of more than three bilayers (*Lavalle 2002, Richert 2002, Halthur 2004-I*). After film assembly, the samples were either dried in nitrogen gas, a procedure which should not affect the film thickness much, or kept in buffer in the QCM-D cells.
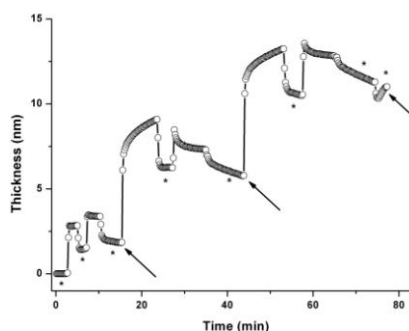

Figure 6.2 *Data from Figure 6.1 was fitted in a Voigt-based model to obtain the adsorbed mass, thus also the film thickness from Equation [5], for each consecutive layer. Each arrow indicates one adsorbed PLL/PLGA bilayer after rinsing with buffer (*). Three bilayers were assembled.*

6.2.3 PLL/PLGA nanofilm assembly studied with ellipsometry

The thickness of the gold surface was measured by ellipsometry, and the raw data were fitted to the calculated data models in the TFCompanion software. A gold thickness of the substrate of 406 ± 7 Å was obtained, which agreed with the 410 Å specification from the supplier. The next step was the SAM surface on gold, which with a simple two layer model was approximated to 18 ± 2 Å. The deposited PLL/PLGA bilayers were modeled both as individual bilayers (SAM-Au-PLL/PLGA, SAM-Au-(PLL/PLGA)$_2$, *etc.*) and as one "single" component (Au-SAM-(PLL/PLGA)$_3$). However, no models showed an appropriate fit to the measured data. Consolidating that the film not was rigid, air was included in both models. Incorporation of 10 vol% air gave a very good fit to the measured data when modeled as one single component. The dry

film thickness then resulted in 40 ± 3.4 Å. The mean square error for such a fit was 0.011 for all measurements. Together with the information about the wet film thickness received from the QCM-D measurement, *i.e.* 10 nm, the results indicated that about 60 % of the wet film consisted of water. Such water content is in agreement with literature values. However, in this study the PLL/PLGA film was assembled without the use of a primer. For the intended application, this is a considerable advantage because of the toxicity possessed by some of the commonly used primers.

6.3 PLL/PLGA *2D* nanofilms exposed to enzymes

In the Theory section it was mentioned that the pH is elevated in chronic wounds (*Dissemond 2003*). Chemical hydrolysis of the film components at pH 7.4 can be assumed to be negligible, and only enzyme catalyzed degradation should occur. Also, the temperature was increased during degradation studies in the QCM-D to simulate skin temperature. The substrate specific V8 protease from *S. aureus* will also have an increased activity at this pH and temperature. An optimum film degradation time would be rather short if used as drug delivery barrier for infection. Thus, it would be of interest to have a release within 24 hours.

6.3.1 Enzymatic degradation studied with QCM-D at skin temperature

The Peltier plate was set to 32 ^{o}C. Important to note was that the system's real temperature was 30.4 ^{o}C, since the Peltier plate proved not to be accurate at higher temperatures. However, since the skin temperature varies between 26 and 36

^{o}C, the slight lowering of the temperature was considered to be acceptable for the intended application. As described in Chapter 3.5.2, the serine protease HNE (human neutrophil elastase) is naturally present in all wounds and destroys bacteria and damaged tissue as part of the healing cascade (*Heck 1985, Korkmaz 2007*). Hence, HNE was used as reference enzyme for simulation of non-infectious wounds. After injection of HNE, the QCM-D measurements revealed a slight increase in frequency, which can be related to the enzymatic adsorption to the film surface. This behavior is an initial step that can be seen in enzymatic degradation profiles; however, further measurements with HNE showed no increase in frequency, indicating no degradation of the (PLL/PLGA)$_3$ film. The same procedure was repeated with the second reference enzyme, trypsin, and similar results were obtained as with HNE. Making sure the enzyme was active and attached to the substrate, trypsin was sequentially injected into the QCM-D chamber. This resulted in a stepwise increase in frequency, indicating progressive adsorption of trypsin. Both reference enzymes were initially added at low concentrations (1:100), similar to that present in a chronic wound; however, due to the high price of HNE, only trypsin was employed in higher concentrations. Addition of HNE resulted in an increase in film layer thickness of only a few nm, while the thickness of the adsorbed trypsin depended on the enzyme concentration injected into the measurement chamber. In both cases no enzyme catalyzed film degradation was observed over time. Studying the dissipation of the two different reference enzymes it was found that ΔD increased slightly. The increase in film softness was probably due to entrapment of solvent

during and after adsorption; however, a partial degradation of peptide bonds, which would be expected to soften the film without fully degrading it, is also conceivable. The results described above were important for the intended application, especially since both enzymes carry a net negative charge at pH 7.4, which triggers adsorption to the positively charged PLGA. The situation was very different with the glutamyl endopeptidase, however. After injecting it into the measurement chamber the frequency increased almost immediately. This increase in Δf indicated loss in mass and hence degradation of the PLL/PLGA film. The graph shown in Figure 6.3 has stitched QTools files describing the desorption of film constituents at 30.4 ^{o}C. There is an obvious change in film properties with increased temperature, *i.e.* swelling. Thus, swelling of the PLL/PLGA nanofilm with increased temperature complicated the quantitative interpretation of the residual film thickness, if any. The first and strongly adsorbed PLL layer, or parts of it, may be thin and rigid and hence able to withstand or delay detachment (*Bingen 2008, Suchy 2011*). Also, the swelling of the film with increased temperature may have concealed the remaining thickness after degradation. In order to assure that the presence of active enzymes was not the limiting factor more V8 was injected into the cell. This did not result in any further loss of material, however. The degradation profile is presented in Figure 6.4. The initial enzymatic adsorption step is seen as the first sharp peak (increased thickness), at the same time as the dissipation increased due to softening of the film. The increase in D is a sign of enzymatic activity due to cleavage of peptide bonds, *i.e.* softening of the film by allowing more solvent into the polymer network. In the

second step a considerable amount of mass was lost. It is conceivable that the soft PLL and PLGA layers intermingled in 3D networks, exposing parts of the underlying polyelectrolyte layers. Such a rearrangement would enable new PLGA segments to be exposed as the proteolytic activity proceeds (see Chapters 3.1.1 and 3.1.2). The desorption continued until reaching a plateau, which indicated complete, or near complete, degradation of the nanofilm.
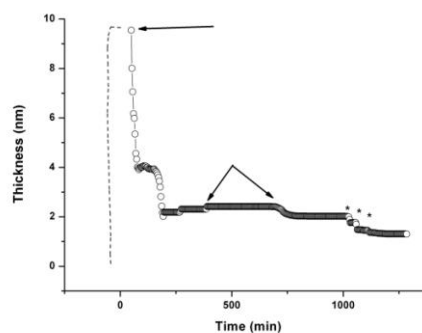

Figure 6.3 *The graph describes the enzymatic degradation of the PLL/PLGA nanofilm. The film assembly is schematically presented by the dashed line (for details see Figure 6.2). The first arrow (left) indicates the addition of glutamyl endopeptidase (V8), which also is the start of the enzymatic degradation. Simultaneously, the temperature is changed from 22.5 to 30.4^{o}C. The two arrows in the middle of the graph indicate addition of more V8, which was made to study whether the film could be further degraded and * indicates the final rinsing steps using Milli-Q water.*
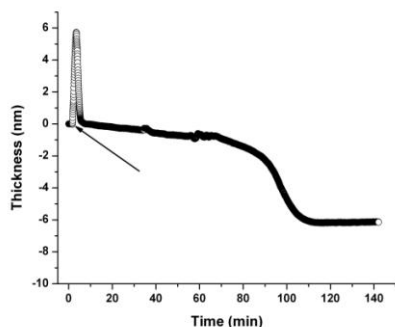
Figure 6.4 *The enzymatic degradation profile. Substrate specific V8 enzyme was added (arrow) and adsorbed readily to the PLL/PLGA film surface, hence initially increasing the film thickness. The adsorption leads to proteolytic activity and degradation of the nanofilm. The graph does not include rinsing steps, see Figure 6.3.*

All the above measurements were performed with three bilayers and PLGA as the terminating layer, making sure that glutamic acid bonds were exposed to the V8 protease. Additionally, tests using V8 on a film with PLL as the final layer was also investigated. The film consisted of three layers, *i.e.* 1.5 bilayers. The QCM measurements indicated that the negatively charged V8 enzyme adsorbed readily to the cationic PLL. However, no degradation was observed. This behavior was expected, since the bacterial enzyme is known to primarily cleave Glu-X bonds. Thus, for enzymatic degradation to occur, PLGA needs to be exposed to the enzyme.

6.3.2 Enzymatic degradation studied with ellipsometry at ambient temperature

The enzymatically treated (Au-SAM)-(PLL/PLGA)$_3$ samples were measured in the same way as the film assembly, but with addition of yet another layer with 10 vol% air during the fit of the model. The temperature during the enzymatic exposure was set to 25 ^{o}C. As expected, trypsin adsorbed readily to the nanofilm, which

resulted in a 5-fold increase of the film thickness at room temperature after 16 hours as seen in Figure 6.5. V8 behaved differently under the set conditions. The (PLL/PLGA)$_3$ thickness was more or less unchanged after addition of the V8 enzyme (Figure 6.5), despite the known attraction between the enzyme and the Glu-X bond. This implies that there is no interaction between V8 and the nanofilm at room temperature. This was an important piece of information, since it indicates that the nanofilm would stay intact and store covered antimicrobial substances until in contact with a wound at skin temperature. Although no direct difference in thickness was observed, it was concluded that the film surface exposed to V8 proteases had been subject to a slight proteolytic activity as evidenced by an increased surface roughness of the polypeptide film. However, the increased surface roughness ($\pm$ 6 Å) disappeared with time, *i.e.* 24 to 48 hours, when all measuring points ended up at the same value ($\pm$ 1 Å).
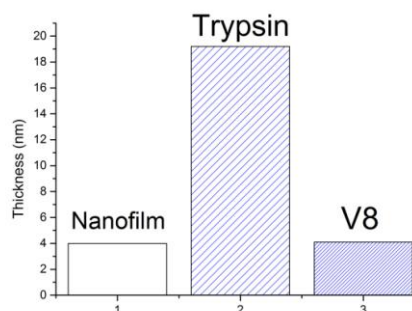

Figure 6.5 *The dry nanofilm had a thickness of 4 nm after three PLL/PLGA layers. The thickness increased significantly when exposed to trypsin (after 16 hours); however, the V8 enzyme had little effect on the layer thickness at ambient temperature.*

6.4 Polyelectrolyte shells as barriers of *3D* nanofilms

The use of a polyelectrolyte film as a barrier carrying a drug can be realized when applied as a shell around the drug, or alternatively with the drug incorporated in the shell. In this section microspheres and microcapsules have been assembled with shells responding to different bacterial proteases.

6.4.1 o/w emulsion based microspheres

The idea of microspheres with an oily core originated when handling the easily hydrolysable betaine ester; however, it was also seen as an opportunity to incorporate hydrophobic drugs in the oil phase. The betaine ester was only soluble in a polar oil (glyceryl trioctanoate (GTO)). The o/w emulsion with a betaine ester/GTO core and a polypeptide shell produced rather stable emulsions. As for visualizing the event, the model drug Nile Red was dissolved in a GTO/corn oil mixture, since pure GTO in combination with Nile Red produced an emulsion with poor stability. For both types of spheres, PLGA was used as emulsifier, followed by the LbL assembly with oppositely charged PLL, and so on, until up to 5 layers were assembled. For each layer, the ζ-potential was measured, see Figure 6.6. The wash step was tedious and gave a low yield, particularly with pure GTO and betaine ester as the core, since the density of water and GTO are very similar. High speed centrifugation, sufficient to separate the droplets from the water phase, but not violent enough to rupture them, seemed to be the best solution. Filtration was investigated, but it resulted in clogged membranes and ruptured spheres. (PLGA/PLL)$_{2.5}$ microspheres with a

diameter of 1-3 μm can be seen in Figure 6.7. To improve the o/w emulsion stability, the polypeptides were crosslinked with EDC and sulfo-NHS without considerable change in sphere size. The concentration of both agents were varied and 200 mM EDC and 50 mM sulfo-NHS were found to be optimal for good stability over time.
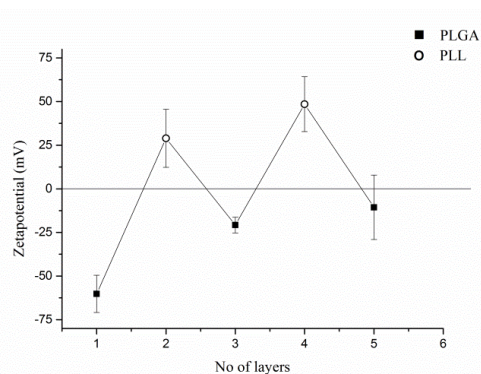

Figure 6.6 *ζ-Potential of the microspheres after stepwise adsorption of PLGA and PLL. Error bars represent standard deviations calculated from three experiments.*
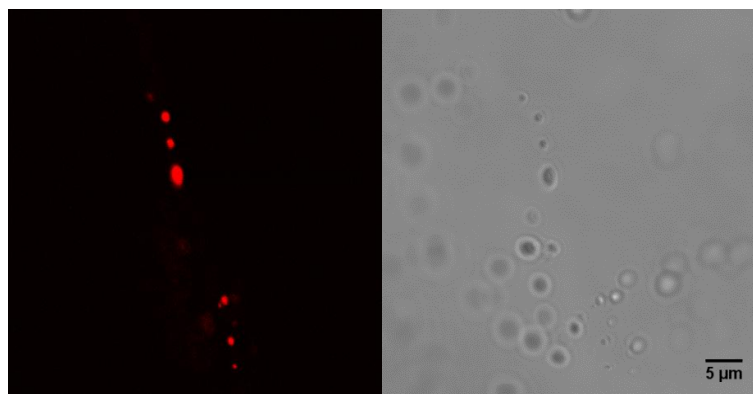

Figure 6.7 *Left: CLSM picture of microspheres. The red color depicts the core loaded with Nile red dissolved in a 1:1 mixture of GTO and corn oil. The nanofilm acting as shell consists of 2.5 crosslinked bilayers. Right: A light microscope picture revealing the real amount of microspheres in the same frame.*

The emulsions with crosslinked shells showed very little separation after more than one year on a magnetic stirrer. However, when the microspheres were placed in an ESEM for evaluation at 1 ^{o}C and approximately 657 Pa, the spheres resisted the "harsh" conditions until the water had fully evaporated from the polypeptide shell, a process which first flattened and then ruptured the spheres (see Figure 6.8). Prior to the evaporation, the picture quality was very poor.
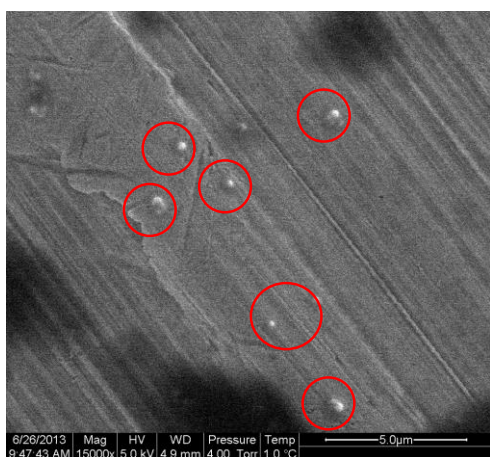

Figure 6.8 *The ESEM picture shows dried o/w microspheres with a PLGA/PLL-shell and are circled for better visibility. Focusing the beam destroyed the spheres, which made it difficult to receive high resolution pictures. The drying process partly flattened the microspheres, which made them look smaller in their dry state than in solution. (Anna Jansson, Applied Physics, Chalmers University of Technology)*

6.4.2 Microspheres exposed to enzymes studied with CLSM and UV/vis

The enzyme solutions were added to the microsphere solutions for 16 hours at 32 ^{o}C

in concentrations of 1:8 for HNE and 1:50 for V8 to investigate the proteolytic degradation on crosslinked spheres. The HNE concentration was a test for stability in an extreme situation and the V8 concentration was within the range of an infected chronic wound. As a first step, CLSM was used to study the effect of the proteases.

HNE had an effect on aggregation of the spheres (Figure 6.); however, the fluorescent probe was still present in the oily core. Thus, no release was discovered when exposed to HNE. As for the samples with added V8, no microspheres were anywhere to be found. The search led to the edge of the sample droplet, where the release of Nile Red was driven onto the glass surface, avoiding the hydrophilic buffer, see Figure 6.10.
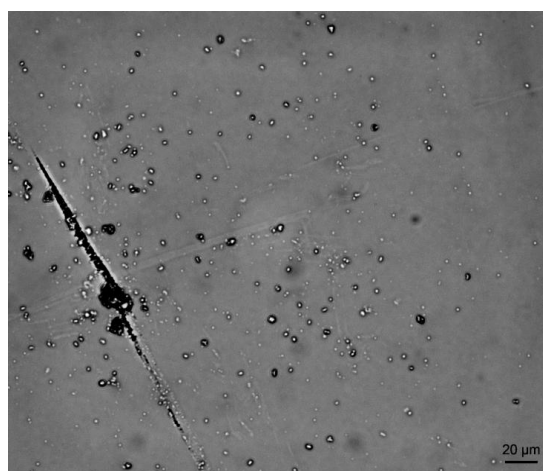

Figure 6.9 *Microspheres after addition of HNE at 32 ^{o}C for 16 hours. The microspheres are intact, although slightly more aggregated, particularly around the piece of dust to the left.*
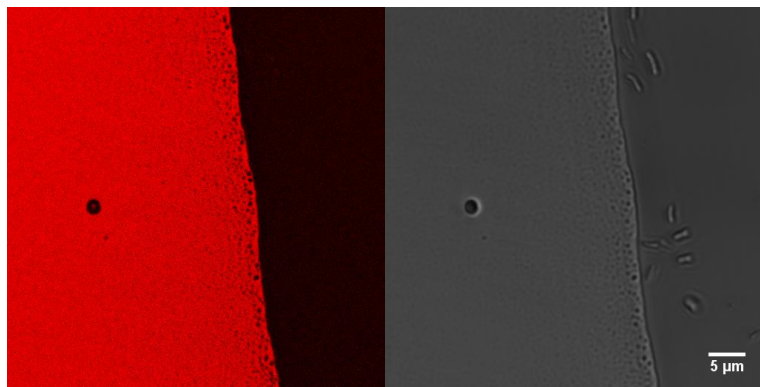
Figure 6.10 *After adding V8 protease, the microspheres degraded leaving only a few polymeric aggregates in solution. The hydrophobic Nile red was either found in these aggregates or adhering to the glass surface (left).*

To further support the idea about release of Nile Red from the microspheres after exposure to V8, isopropyl myristate (IPM) was chosen as release medium and UV spectroscopy as detection method. Nile Red has very low solubility in water (1 µg/mL) (*Castro 2005*) and would not give reliable release results. For the standard curve, see Paper III. A rapid release during stirring was found at 32 ^{o}C and only within a couple of hours a maximum had been reached at 0.13 mM, see Figure 6.11. This concentration is equivalent to 41.4 µg/mL in the microsphere suspension, which is a relevant drug dosage. Also a higher concentration could be achieved by increasing the microsphere concentration in the dispersion. However, since the concentration after 24 hours was slightly lower, 0.10 mM, either a gradient may have created the maximum, or the stirring was too weak to prevent Nile Red from adsorbing to surrounding hydrophobic surfaces.
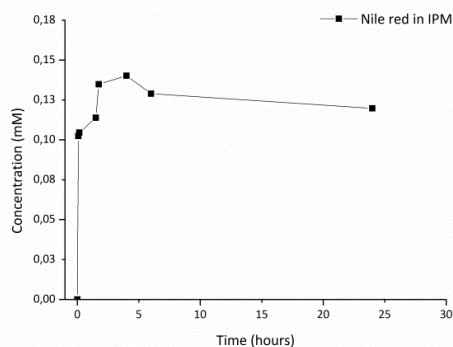

Figure 6.11 *Release curve of Nile red in IPM during 24 h.*

6.4.3 PAH/PLGA assembly with CaCO$_3$ as sacrificial template

The porous CaCO$_3$ template had a size of approximately 3 µm with a pore size of below 10 nm (personal communication, Plasmachem GmbH). CaCO$_3$ spheres in the range of 4-6 µm usually have pores in the range of 20-60 nm (*Volodkin 2004*). The pores can either be loaded with active substance prior to the LbL assembly or by postloading. Due to the bulkiness of one of the drugs and due to aggregation issues of the templates in the absence of a polyelectrolyte layer, the last approach was used. The CaCO$_3$ spheres were negatively charged at pH 7 (-40 mV); however, both anionic and cationic polyelectrolytes could be deposited onto the templates (personal communication with supplier). In order to

achieve good coverage of the pores, PAH, which is a high molecular weight polyelectrolyte, was chosen for the initial layer. High molecular weight polysaccharides had previously been used for the same purpose (*Szarpak 2008*). Although a high MW PAH was used as the first layer, the PLL/PLGA system did not seem to provide enough coverage for the subsequent layers, and severe aggregation occurred after 2 assembled bilayers. Most likely the molecular weights of the combined polypeptides were too small. Hence, PAH was used as the cationic polyelectrolyte throughout the LbL assembly. PLGA was maintained as the negatively charged polyelectrolyte, due to the specificity of the bacterial protease. It has been reported that capsules should be assembled with maximum 5 bilayers to avoid severe aggregation (*Szarpak 2010*), which also was seen in this study. Hence, the capsules were assembled with 3 bilayers, (PAH/PLGA)$_3$, and the ζ-potential is presented in Figure 6.12. A light microscope was used to keep track on aggregation and to assess the size of the capsules.
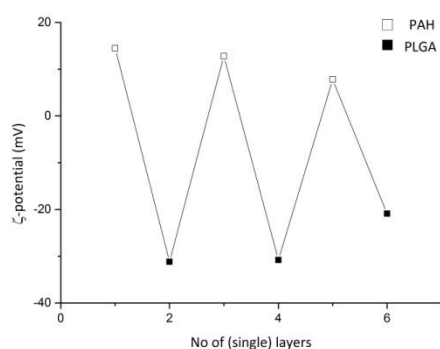

Figure 6.12 *The ζ-potential for each PAH- and PLGA-layer. Three bilayers were assembled, (PAH/PLGA)$_3$.*

Crosslinking the film by addition of EDC and sulfo-NHS led to aggregation. After dissolving the template core by addition of GDL, the light microscopy and ESEM pictures showed finely dispersed capsules. A tentative explanation to the aggregation is a change in surface charge on the microcapsules after crosslinking. Some amino groups and carboxyl groups have been transformed into amide bonds, which mean that the concentration of charged functional groups on the capsule surface has decreased. This may lead to reduced electrostatic stabilization of the dispersion. However, the dissolution of the template led to a high concentration of Ca^{2+} ions, resulting in the increase of the electrostatic repulsion due to a screening effect. Also, throughout the work, it was seen that the microcapsules readily aggregated at very low or very high ionic strengths, while a salt concentration of 0.15-0.5 M NaCl maintained dispersed capsules. The removal of the core could be monitored by the eye, since the suspension turned transparent after GDL addition. This was also confirmed by SEM and one representative picture can be seen in the top of Figure 6.13. In Figure 6.14 a SEM close-up of a whole microcapsule is seen, with its shell interacting with the rest of the clusters' capsule shells in vacuum. This interaction was possibly a reason to why many capsules in clusters did not rupture (in vacuum) while single capsules and a few on the outer parts of the clusters did. Adding EDC at 100 or 200 mM to PAH/PLGA capsules did not result in any visible changes when zooming into the clusters. However, there were many larger clusters, and thus more complete capsules, when EDC had been added in a concentration of 200 mM.
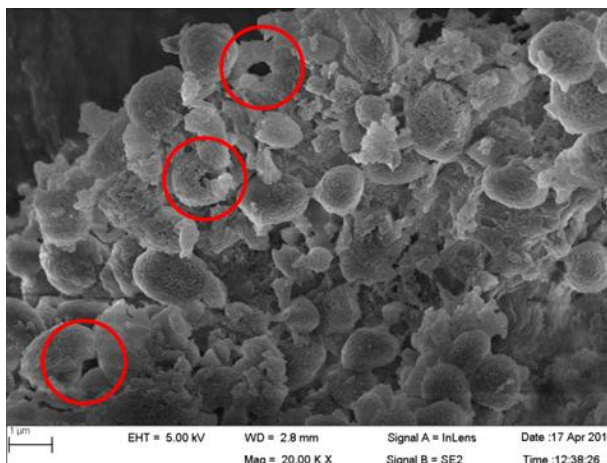
Figure 6.13 *SEM picture of (PAH/PLGA)₃ microcapsules. The harsh environment ruptured single capsules and capsules on the surface of the cluster. In the top of the micrograph, one of the capsules with a damaged shell visualizes the hollow core.*
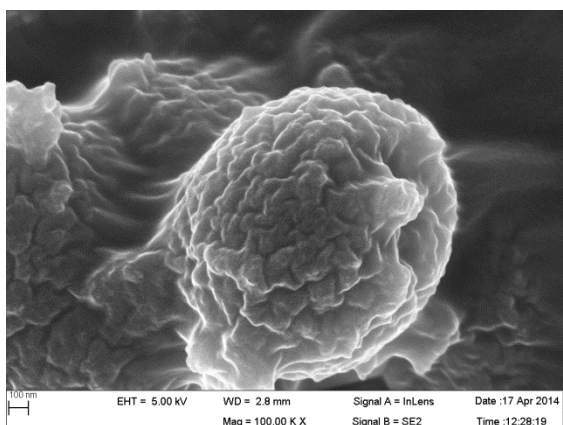

Figure 6.14 *A SEM image close-up of a microcapsule. It can also be seen that the shells in the cluster of capsules interacted during drying in the vacuum, possibly contributing to them not rupturing.*

6.4.4 HA/PLL assembly with CaCO₃ as sacrifical template

The HA/PLL microcapsules were assembled in the same manner as in Chapter 6.4.3. The high viscosity of HA required some small changes in the procedure, which are described in the Experimental section. The choice of hyaluronic acid as anionic polyelectrolyte

was not only due to its non-toxic properties, but also to its availability in high molecular weights, which is important for good coverage of the $CaCO_3$ pores. The ζ-potential for the HA/PLL film build-up is presented in Figure 6.15. HA is a sticky macromolecule with good wetting ability, which allowed the $(HA/PLL)_3$ shell to swell in solution (*Knepper 1995, Nitzan 2001, Scherge 2001*). Hence, the crosslinked and hollow microcapsule average size ended up between 3 and 5 μm in diameter. Again, it was obvious that the core became hollow after addition of GDL as the solution changed from milky to transparent. This was also visualized with SEM, see Figure 6.16, which shows a sample that has been crosslinked with 100 mM EDC, a concentration which only gave a few capsules that were more or less intact (in vacuum).
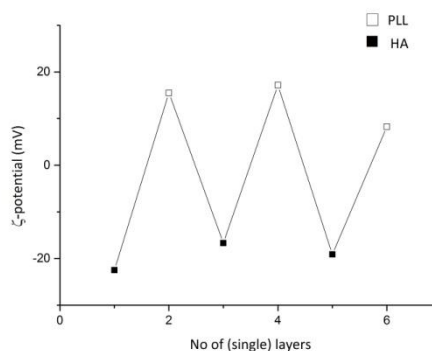

Figure 6.15 *The ζ-potential for each HA- and PLL-layer. Three bilayers were assembled, $(HA/PLL)_3$.*
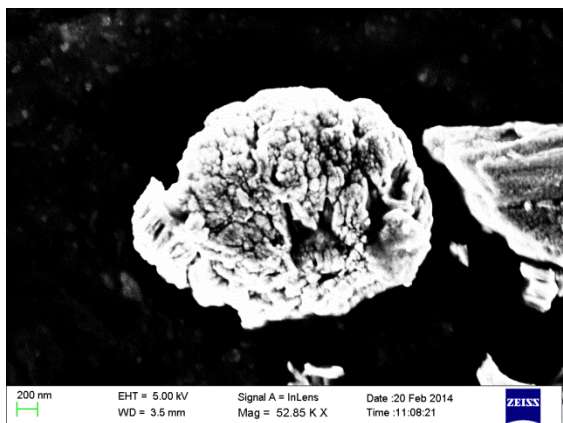
Figure 6.16 *SEM image of a crosslinked (100 mM EDC/50 mM Sulfo-NHS) and hollow (HA/PLL)₃ that ruptured in vacuum. Most capsules had ruptured in vacuum.*

By increasing the EDC concentration the shell remained intact, but the capsule instead collapsed in the center, see Figure 6.17.
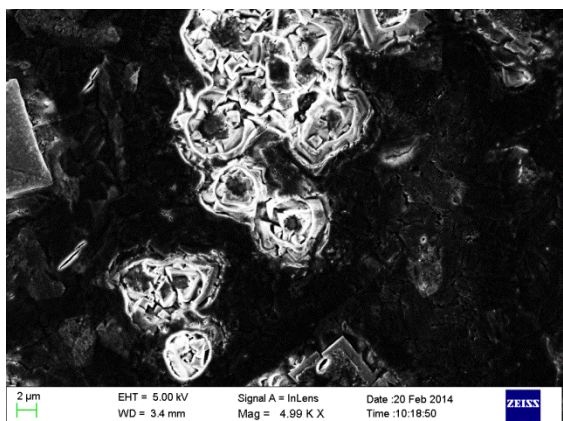

Figure 6.17 *SEM image of crosslinked (200 mM EDC/50 mM Sulfo-NHS) (HA/PLL)₃ capsules. The high EDC concentration gives an intact shell; however, the top has collapsed.*

Similar to the PAH/PLGA capsules the polysaccharide containing capsules did not cope with vacuum. More or less all HA/PLL capsules collapsed or ruptured in vacuum; however, as air-dried PAH/PLGA and HA/PLL capsules were complete after air-drying (studied with light and fluorescence microscopy), the ruptures seemed to be related to the harsh

conditions under the preparation of the SEM samples and in the SEM.

6.4.5 Loading of PAH/PLGA and HA/PLL microcapsules

The loading of the microcapsules with FITC-dextran is described in Paper IV-V and in the Experimental section. FITC-dextran is used as a model drug to show proof of concept in loading the two capsule types with an available and equitable probe. The PAH/PLGA capsules ended up with a fluorescence about twice as high as the background intensity, which was unwashed and still contained the probe solution. Similarly, the HA/PLL capsules resulted in an intensity 1.5 times higher than the background (see Paper V). These results indicated successful FITC-dextran loading of both capsule types; however, the loading of the HA/PLL capsules was time-dependent. Instead of 30 minutes loading time as for PAH/PLGA capsules, several hours were needed for the polysaccharide containing capsules. This slow step was possibly related to the very large anionic HA molecule creating an obstacle for penetration through the film for the anionic probe. On the contrary, when drug-like probes were used, *i.e.* Rhodamine Green and Vancomycin BODIPY, both capsule types could easily be discovered in the microscope due to a stronger intensity in the loaded capsules compared to the background. After loading the actual drugs, PHMB and Vancomycin, the suspensions were put through a syringe filter. By doing so, the drug content of the microcapsules could be indirectly estimated by NMR by measuring the remaining drug concentration in the surrounding solution. As was indicated with microscopy for the capsules with the drug-like probes, a large quantity of drug had disappeared from the solution. 80 % of PHMB or 50 % of

Vancomycin were present in the PAH/PLGA capsule structure, while the HA/PLL capsules contained 80 % PHMB and 20-40 % Vancomycin. Continuing measurements with NMR on the washed capsule suspensions indicated that PHMB and Vancomycin were mainly immobilized in the capsule shell. Additionally, independent of which drug that was used, about 1 % of drug adsorbed to the outer capsule wall was in equilibrium with the surrounding solution, see Table 6.1.

Microcapsule and drug	Pure solution: Encapsulated drug conc [drug in equilibrium] (mg/mL)	AM test samples (dilution): Encapsulated drug conc [drug in equilibrium] (mg/L)
(HA/PLL)$_3$ + PHMB	24 [0.15]	12 [0.075]
(HA/PLL)$_3$ + VAN	0.60 [0.015]	0.30 [0.0075]
(PAH/PLGA)$_3$ + PHMB	24 [0.15]	12 [0.075]
(PAH/PLGA)$_3$ + VAN	0.70 [0.015]	0.35 [0.0075]

Table 6.1 *Concentrations of encapsulated PHMB and Vancomycin (VAN) and the surrounding drug in equilibrium in brackets as determined with NMR. The right column displays the actual concentrations during the antimicrobial tests after dilution with bacteria in SWF. (Note: The HA/PLL microcapsule batch with VAN in the table had a loading capacity of 40 %.)*

6.4.6 PAH/PLGA and HA/PLL nanofilms exposed to enzymes

CLSM, light microscopy and NMR were the techniques used to evaluate the effect of enzymatic exposure of the microcapsules. Particularly CLSM was used to visualize and measure any change in microcapsule structure and intensity before and after enzymatic exposure. Additionally, with FITC-dextran as the fluorescent model drug it was possible to detect whether it was released or if it remained in the capsule after exposure to proteolytic enzymes. Capsules exposed to the human wound enzyme, HNE, did neither rupture the capsule structure nor release the probe, see Figure 6.18. Unfortunately, the picture quality for the HA/PLL images ended up poor due to problems with the zoom, hence a microscopy image of the same sample was taken using a light microscope (Figure 6.18 (c)). Figures 6.19 (a) and (b) show the PAH/PLGA capsules loaded with FITC-dextran before and after addition of V8 protease at 32 $^{\circ}$C. Figure 6.20 (a) and (b) describe the HA/PLL capsules before and after addition of Protease IV. Both capsule types exposed to their respective bacterial proteases released all the anionic probe; however, since the samples were unpurified, a small amount of probe was still found in the structures when measuring the intensity before and after enzymatic exposure (Figure 6.21). In short, in a clean environment V8 degraded the Glu-X bonds and Protease IV cleaved Lys-X bonds, thus exposing the anionic probe successfully. Since V8 and Protease IV are bacterial virulence factors, the initial results indicated that a release related to the degree of infection can be achieved. Hence all results above were in accordance

with the results presented in Chapter 6.3.1. The FITC-dextran signal was unfortunately not strong enough for investigation of the release by NMR but both PHMB and Vancomycin were easily detectable.
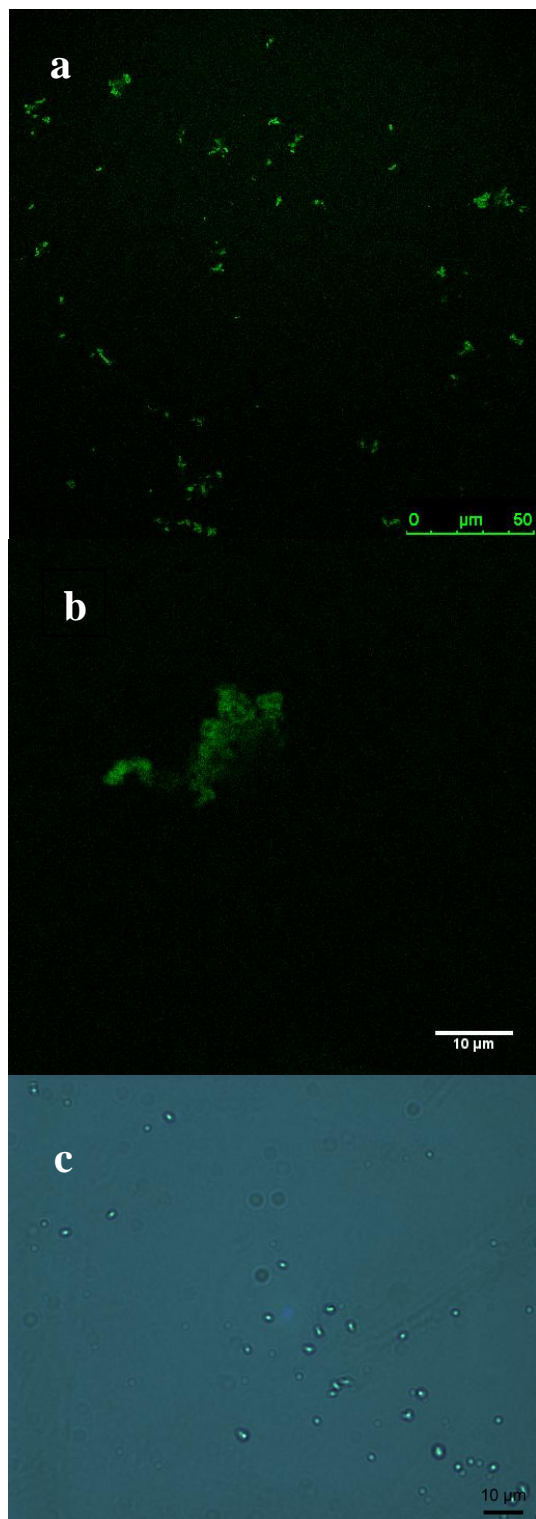

Figure 6.18 *CLSM images after exposure to HNE. (a) PAH/PLGA capsules are still intact with the*

probe present in the capsules. (b) HA/PLL capsule images ended up poor; however, (c) shows a light microscopy image of the sample. Together, (b) and (c) indicate that the capsules are intact and that the probe is present in the capsules. HNE did contribute to a slight aggregation of HA/PLL capsules.
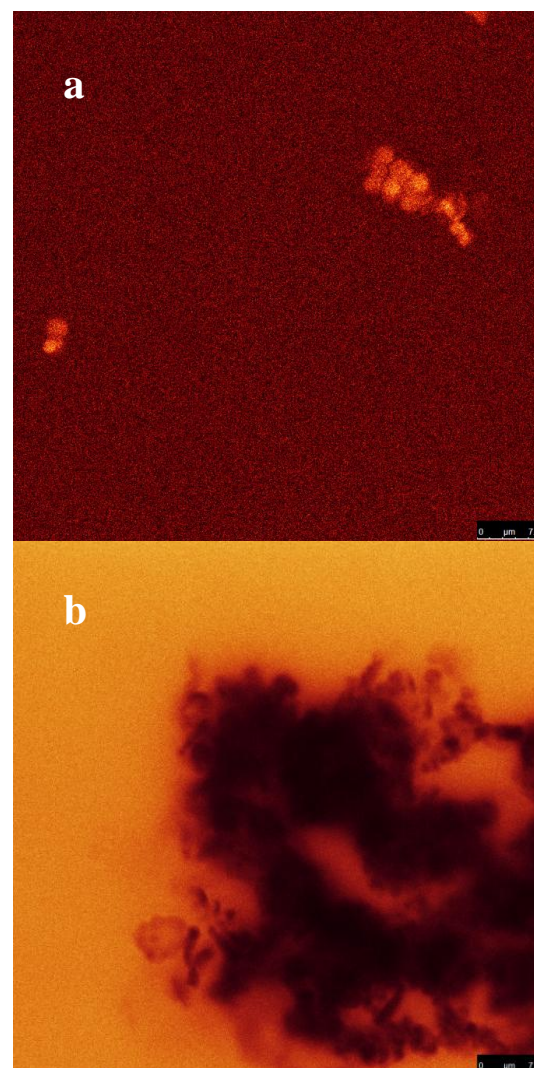

Figure 6.19 *PAH/PLL microcapsules with FITC-dextran in (a) and after exposure to V8 in (b).*

As previously described, both PHMB and Vancomycin were mainly immobilized in the capsule structure. Despite the efforts of either exposing the loaded capsules to the bacterial proteases in a shaker at 32 °C or adding the proteases straight into the NMR

tube at 32 ^{o}C before the measurement, all samples ended up with drugs still bound to the degraded structures. However, light microscopy and CLSM images confirmed the rupture of both the PAH/PLGA and the HA/PLL microcapsules after exposure to V8 and Protease IV, respectively.
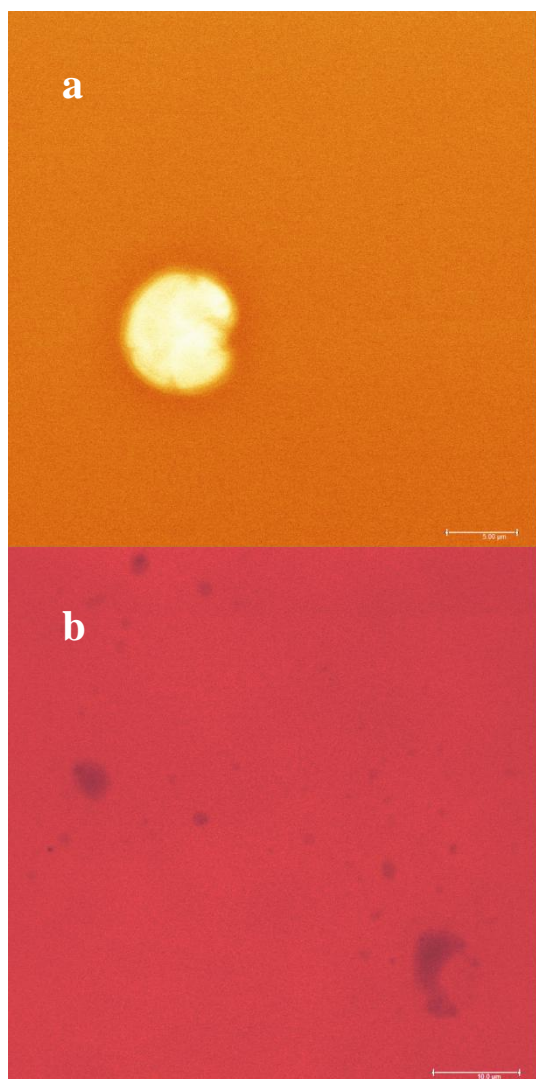

Figure 6.20 *Image (a) shows a single HA/PLL capsule loaded with FITC-dextran. In (b) the exposure to Protease IV has degraded the capsule structures and the probe is released.*
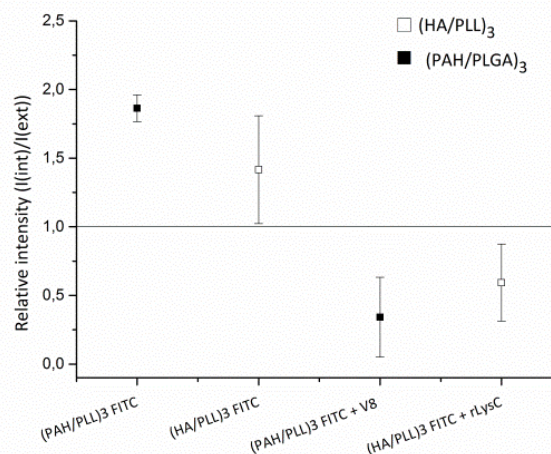

Figure 6.21 *The intensity was measured in the CLSM images. Relative intensity (with the background (external) intensity set to 1) for the two types of microcapsules. The (PAH/PLL)₃ microcapsules went from 1.8 to 0.4 after exposure to V8. The (HA/PLL)₃ microcapsules went from 1.5 to 0.6 after exposure to Protease IV (named rLys-C in the figure).*

6.4.1 Antimicrobial efficacy of microcapsules

A buffer solution is a much different environment than a wound fluid. Instead, a protein rich solution called simulated wound fluid, SWF, can be used. Such an environment is much closer to reality, but the chemical analysis of drugs and their release in SWF is intricate. However, SWF is also used as a nutritious medium for bacteria, allowing the antimicrobial (AM) effect of the drug release to be investigated by studying the survival of the microorganisms. The solution's protein content will act as a physical hinder between the enzymes and the capsules as well as the drugs and the bacteria, resulting in a much tougher test than in a buffer solution. The microorganisms chosen were two virulent strains originating from wounds, i.e. *Staphylococcus aureus* and *Pseudomonas aeruginosa*. Both capsule types were either empty or loaded with

PHMB or Vancomycin. Also, as described earlier, 1 % of the loaded drugs were in equilibrium with its surroundings. Hence, samples containing free PHMB or Vancomycine in buffer were also tested on the two bacteria. In the current AM study a successful killing effect was related to a log-reduction of 4, *i.e.* to 10^2 in bacterial count, which is the same as the detection limit for the current method. Such a decrease normally assures that the infection is eliminated and that no regrowth of the treated colonies will occur. As can be seen in Figures 6.22 and 6.23, the free roaming PHMB had an immediate killing effect on both *S. aureus* and *P. aeruginosa*, and the bacterial count was lowered to below the detection limit only after 3 hours. Vancomycin had as expected no effect on *P. aeruginosa.* On *S. aureus* it had a slight effect after 3 hours and an insufficient killing effect after 24 hours (10^3). With these results it may have seemed unnecessary to test the loaded microcapsules on bacteria. However, an environment with immobilized drugs in the microcapsules is rather different from one with freely diffusing drug molecules and the outcome of the AM test with the microcapsule dispersion is therefore not easy to predict.

When the PAH/PLL capsules containing the bulky antibiotic substance was added to *S. aureus*, the AM effect was small after 3 hours, but landed on a count below the detection level after 24 hours. Thus, in this form the microcapsule allowed for a successful killing effect compared to the result with the pure Vancomycin solution, most probably due to a burst release effect as a result of V8's proteolytic activity. This also confirms that the capsule environment is very different from that of the free drug in solution. Interestingly, Vancomycin in

HA/PLL capsules also killed *P. aeruginosa* within 24 hours. This was somewhat unexpected considering that *P. aeruginosa* is a Gram-negative species. As mentioned in the Theory section, Vancomycin is generally not active against Gram-negative bacteria, which also was seen with free Vancomycin in solution. Surface active agents or acids can increase the permeability of the bacterial membrane and hence work as a synergist and increase the antimicrobial effect of an antibiotic substance (*Ayres 1999*). Also, recent studies have shown an enhanced antimicrobial effect due to stronger interaction with the bacterial membrane on *P. aeruginosa* using Vancomycin, which was adsorbed or covalently bound to a carrier particle or molecule (*Kell 2008, Gurunathan 2014*). In the present communication we did not study this surprising mechanism further, although there was obviously an element of synergistic nature increasing the efficacy of Vancomycin against the Gram-negative species. The enzymatic degradation of the nanofilm by Protease IV may have created moieties working as carriers or permeabilizers responsible for the synergistic effect.

When loading the microcapsules with PHMB, a less bulky molecule than the antibiotic discussed above, both microcapsule formulations showed no effect on any bacterium after 3 hours, but a successful killing effect after 24 hours. Such results also indicate that the capsule suspensions should not be compared to a drug without a carrier. The strong antimicrobial effect of free PHMB in solution is believed to be related to the relatively high content of free PHMB in solution. Contrary to Vancomcyin loaded capsules, the PHMB molecules

surrounding the microcapsules could not be disregarded when evaluating the antimicrobial effect related to degradation of the microcapsules.

To investigate the specificity of the bacterial proteases and the nanofilm shells, the microcapsule suspension was added to the "opposite" bacterium, *i.e.* PAH/PLGA to *S. aureus* and HA/PLL to *P. aeruginosa*. The microcapsules were loaded with Vancomycin instead of PHMB, due to the inability of disregarding the effect of the latter drug in solution. The *P. aeruginosa* was unaffected by the PAH/PLL capsules, which was no surprise because of the properties of the drug but also due to the film composition. *S. aureus*, on the other hand, was only slightly affected by the HA/PLL/Vancomycin capsules. This result seems primarily to be due to an inability of *S. aureus* to degrade the nanofilm. The inhibition in growth and the slight decrease was probably due to the drug present in solution.
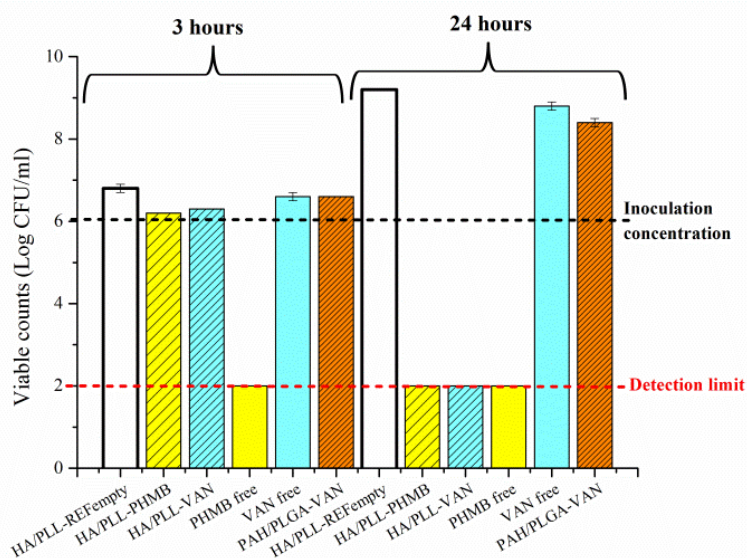

Figure 6.22 *Antimicrobial efficacy against Pseudomonas aeruginosa of free Vancomycin and PHMB and of these antimicrobials loaded into capsules. Simulated wound fluid was used as medium.*

Contrary to FITC-dextran being released from the degraded capsule structures (CLSM), the NMR results for the drugs revealed no release of PHMB or Vancomycin. It was hence clear that the majority of the actives had adsorbed to the nanofilm structure, and stayed immobilized after the proteolytic activity. Also, the drug present in solution was in equilibrium with the surfaces, not roaming free in solution. This means that there are different possibilities to account for the bioavailability of the drugs. The first option is that the drugs are efficient antimicrobials in spite of the fact that they are bound to the degraded polymer. The second option is that the adsorbed drugs are in equilibrium with free drug molecules in solution. We favor the second option, since for both drugs the NMR studies revealed a small but constant amount in the surrounding buffer after washing the capsule suspension. Such a system would allow for a burst release of drugs if exposed to large areas of bacterial cell walls, proteins, *etc*.

The post-loading of drugs into the microcapsules was obviously a straightforward experimental procedure; however, particularly for PHMB the method needs to be improved. Adding polyelectrolyte layers after drug loading, or preloading the templates before LbL assembly are examples of possible ways to improve the procedure. For Vancomycin the PAH/PLGA capsules increased the AM effect on *S. aureus*, probably due to burst release since the AM effect is concentration dependent. The surprising AM effect of Vancomycin on *P. aeruginosa* is yet to be explained. With recent studies in mind it seems likely that a synergy between Vancomycin and products from the proteolytic degradation

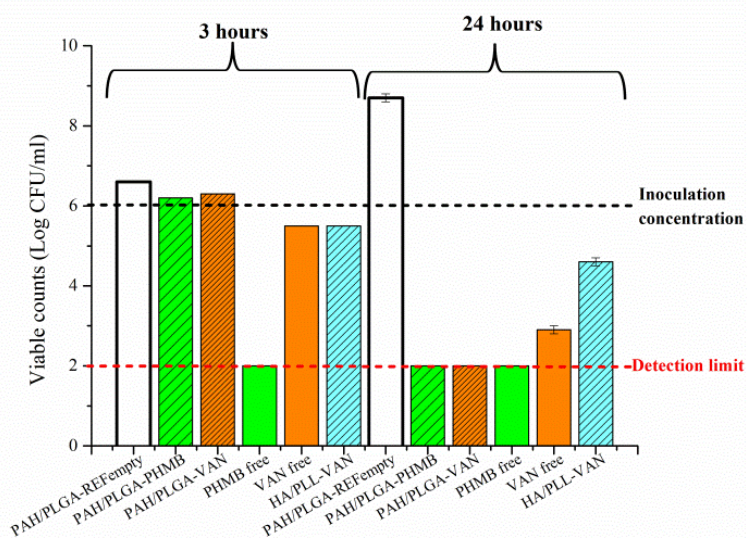of the nanofilm is responsible for the successful killing effect.

Figure 6.23 *Antimicrobial efficacy against Staphylococcus aureus of free Vancomycin and PHMB and of these antimicrobials loaded into capsules. Simulated wound fluid was used as medium.*

7 CONCLUDING REMARKS

By using existing knowledge about drug release, the environment where the drug is released and, in the current work, which microorganisms that can contribute to release, smart release platforms can be assembled. Two bacterial proteases were identified in this project, V8 from *S. aureus* and Protease IV from *P. aeruginosa*. The two enzymes were chosen since they possess the following three characteristics: (1) They are direct or indirect virulence factors; in other words, they exist in pathogens and create disease. (2) They continuously contribute to the survival of the pathogens by providing nutrients through cleaving host tissue. (3) They have a high degree of substrate specificity (which is taken advantage of in peptide mapping). These three characteristics contributed to the idea of creating a nanofilm as a drug barrier, which would degrade only in case of bacterial infection. Such a film would be degraded when a substrate specific virulence factor has reached a certain concentration indicating infection. Hence a smart release system that combats infection, particularly in chronic wounds and only when the drug is needed, could be assembled. V8 is specific for Glu-X bonds, while Protease IV is specific for Lys-X bonds, two peptide bonds that are readily found in polypeptides. Thus, a Glu-X rich bond was created in a *2D* format studied with QCM-D, with PLGA as the anionic component and as the terminating layer. HNE and trypsin were used as reference enzymes; as expected, neither of these degraded the structure, while V8 did. This concept was also applied in "*3D*" as o/w emulsion microspheres and as template assisted assembled (hollow) microcapsules. In those forms, a drug could be incorporated into the structure.

As for Protease IV, a lysine-rich film was assembled in the shape of microcapsules. Initially, an anionic probe was used as model drug. If the nanofilms were crosslinked, their stability against human wound enzymes increased and only a slight aggregation without drug release was discovered. Exposing the same types of microcapsules to the respective protease, the structures were degraded and the model drug released. When loading the microcapsules with a rather large amount of an antimicrobial drug, the result was different. The cationic PHMB and the neutral and bulky Vancomycin were immobilized in the film structures. Using NMR, it was found that before and after degradation of the microcapsules, the amount of drug in the surrounding solution was constant; however, microscopy showed degraded polymeric parts of former capsules. By exposing the microcapsules to bacteria in SWF, the antimicrobial killing effect was evident. For PHMB loaded microcapsules, both S. aureus and P. aeruginosa were eliminated after the specific degradation of the nanofilm shells. However, due to the strong AM effect of the drug, the free drug in the surrounding solution probably also contributed to the antimicrobial effect. On the other hand, for Vancomycin loaded microcapsules, the AM killing effect could be related to the specific degradation of V8 in *S. aureus* and Protease IV in *P. aeruginosa*. However, the antimicrobial effect of Vancomycin on the Gram-negative species was unexpected, but could possibly be related to synergistic effects between the degraded capsule constituents and the drug.

This work involves the assembly of smart delivery systems against infections caused by *S. aureus* and *P. aeruginosa*. By using the bacteria's own survival mechanisms, it was possible to start building a platform for smart drug release that combats infection.

ACKNOWLEDGEMENTS

ACRONYMS

BODIPY	4,4-difluoro-4-nora-3a,4a-diaza-s-indecene
CLSM	confocal laser scanning microscopy
EDC	N-(3-dimethylaminopropyl)-N'-ethylcarbodiimide hydrochloride
ESEM	environmental scanning electron microscopy
FITC-dextran	Fluorescein isothiocyanate-dextran
GDL	gluconoc delta-lactone (D-gluconic acid δ-lactone)
GTO	glyceryl trioctanoate
HA	hyaluronic acid
HNE	human neutrophil elastase
MES	2-(N-morpholino) ethanesulfonic acid sodium salt
NMR	nuclear magnetic resonance
o/w	oil in water (emulsion)
PAH	poly allylamine hydrochloride
PHMB	polyhexamethylene biguanide
PLGA	poly-L-glutamic acid
PLL	poly-L-lysine
QCM-D	quartz crystal microbalance with dissipation monitoring
SAM	self-assembled monolayer
SEM	scanning electron microscopy
Sulfo-NHS	N-hydroxysulfosuccinimide sodium salt
V8	glutamyl endopeptidase
VAN	Vancomycin

REFERENCES

Ahlström, B. (1999-I). Quaternary ammonium esters as soft antimicrobial agents. *Department of Clinical Bacteriology, Gothenburg, Sweden*, doctoral thesis.

Ahlström, B., Thompson, R. A., Edebo, L. (1999-II). The effect of hydrocarbon length, pH, and temperature on the binding and bactericidal effect of amphiphilic betaine esters on *Salmonellatyphimurium*. *APMIS*, *107*, 318-324.

Ahlström, B., Thompson, R. A., Edebo, L. (1999-III). Loss of bactericidal capacity of long.chain quaternary ammonium compounds with protein at lowered temperatures. *APMIS*, *107*, 606-614.

Alandejani, T., Marsan, J., Ferris, W., Slinger, R., Chan, F. (2009) Effectiveness of honey on *Staphylococcus aureus* and *Pseudomonas aeruginosa* biofilms. *Otolaryngol. Head Neck Surg. 141* (1), 114-118.

Azzam, R. M. A., Bashara, N. M. (1987). Ellipsometry and polarized light. *Elsevier, Amsterdam, Holland*, 2nd ed.

Bain, C. D., Evall, J., Whitesides, G. M. (1989-I). Formation of monolayers by the coadsorption of thiols on gold: Variation in the head group, tail group, and solvent. *J. Am. Chem. Soc., 111* (18), 7155-7164.

Bain, C. D., Troughton, E. B., Tao, Y. T., Evall, J., Whitesides, G. M., Nuzzo, R. G. (1989-II). Formation of monolayer films by the spontaneous assembly of organic thiols from solution onto gold. *J. Am. Chem. Soc.*, *111* (1), 321-335.

Beanes, S. R., Dang, C., Soo, C., Ting, K. (2003). Skin repair and scar formation: the central role of TGF-β. *Expert Rev. Mol. Med.*, *5* (8) 1-11.

Bingen, P., Wang, G., Steinmetz, N. F., Rodahl, M., Richter, R. P. (2008). Solvation effects in the quartz crystal microbalance with dissipation monitoring response to biomolecular adsorption. A phenomenological approach. *Anal. Chem.*, *80* (23), 8880-8890.

Bjarnsholt, T., Kirketerp-Moller, K., Kristiansen, S., Phipps, R., Nielsen, A. K., Jensen, P. O., Høiby, N., Givskov, M. (2007). Silver against Pseudomonas aeruginosa biofilms. *APMIS*, *115* (8), 921–928.

Blodgett, K., B. (1934). Monomolecular films of fatty acids on glass. *J. Am. Chem. Soc.*, *56*, 495.

Blodgett, K., B., Langmuir, I. (1937). Build-up films of barium stearate and their optical properties. *Phys. Rev.*, *51* (11), 964-982.

Bordes, R., Höök, F. (2010). Separation of bulk effects and bound mass during adsorption of surfactants probed by quartz crystal microbalance with dissipation: insight into data interpretation. *Anal. Chem.*, *82* (21), 9116-9121.

Bowler, P. G. (1998). The anaerobic and aerobic microbiology of wounds. *Wounds*, *10* (6), 170–178.

Brackman, G., De Meyer, L., Nelis, H. J., Coenye, T. (2013) Biofilm inhibitory and eradicating activity of wound care products against *Staphylococcus aureus* and *Staphylococcus epidermidis* biofilms in an *in vitro* chronic wound model. *J. Appl. Microbiol. 114*, 1833-1842.

Breddam, K., Meldal, M. (1992). Substrate preferences of glutamic-acid specific endopeptidases assessed by synthetic peptide substrates based on intramolecular fluorescence quenching. Eur. J. Biochem., *206* (1), 103-107.

Broxton, P., Woodcock, P.M., Gilbert, P. (1983). A study of the antibacterial activity of

some polyhexamethylene biguanides towards Escherichia coli ATCC 8739. *J. Appl. Bacteriol.*, *54*, 345–353.

Broxton, P., Woodcock, P.M. and Gilbert, P. (1984-I). Binding of polyhexamethylene biguanides to the cell envelope of Escherichia coli. *Microbios., 41*, 15–22.

Broxton, P., Woodcock, P.M., Gilbert, P. (1984-II). Injury and recovery of Escherichia coli from the treatment of polyhexamethylene biguanides. *Microbios.*, *40*, 187–193.

Broxton, P., Woodcock, P.M., Heatley, M., Gilbert, P. (1984-III). Interaction of some polyhexamethylene biguanides and membrane phospholipids in Escherichia coli. *J. Appl. Bacteriol.*, *57*, 115–125.

Burell, R. E.(2003). A scientific perspective on the use of topical silver preparations. *OWM, 49* (5A), 19-24.

Caballero, A., Thibodeaux, B., Marquart, M., Traidej, M., O'Callaghan, R. (2004) Pseudomonas keratitis: Protease IV gene conservation, distribution, and production relative to virulence and other *Pseudomonas* proteases. *Invest. Opthalmol. Vis. Sci.*, *45* (2), 522-530.

Cho, N. J., Kanazawa, K. K., Glenn, J. S., Frank, C. W. (2007). Employing two different quartz crystal microbalance models to study changes in viscoelastic behavior upon transformation of lipid vesicles to a bilayer on a gold surface. *Anal. Chem.*, *79* (18), 7027-7035.

Chung, A. J., Rubner, M. F. (2002). Methods of loading and releasing low molecular weight cationic molecules in weak polyelectrolyte multilayer films. *Langmuir*, *18* (4), 1176-1183.

Craig, M., Holmberg, K., Le Ru, E., Etchegoin, P. (2014) Polypeptide multilayer self-assembly studied by ellipsometry. *J. Drug Deliv.*, *2014*, ID 424697, 5 pages.

Daeschlein, G. (2013) Antimicrobial and antiseptic strategies in wound management. *Int. Wound J. 10* (1), 9-14.

Decher G., Hong J. D., Schmitt, J. (1992). Buildup of ultrathin multilayer films by a self-assembly process: III. Consecutively alternating adsorption of anionic and cationic polyelectrolytes on charged surfaces. *Thin Solid Films*, *210-211* (2), 831-835.

Decher, G. (1997). Fuzzy nanoassemblies: Toward layered polymeric multicomposites. *Science*, *277* (5330), 1232-1237.

Decher, G., Schlenoff, J. B. (2003). Multilayer thin films – sequential assembly of nanocomposite materials. *Wiley-VCH Verlag GmbH & Co. KGaA, Weinheim*, p. 3-4, 6-7, 9, 12, 17-20, 23, 222, 400.

Dissemond, J., Witthoff, M., Brauns, T. C., Haberer, D., Goos, M. (2003). pH values in chronic wounds. Evaluation during modern wound therapy. *Hautarzt*, *54* (10), 959–965.

Dobrynin, A. V., Rubenstein, M. (2005). Theory of polyelectrolytes in solutions and at surfaces. *Prog. Polym. Sci.*, *30*, 1049-1118.

Driver, V. R., Fabbi, M., Lavery, L. A., Gibbons, G. The costs of diabetic foot: the economic case for the limb salvage team. (2010). *J. Am. Podiatr. Med. Assoc.*, *100* (5), 335–341.

Dubas, S., T., Schlenoff, J., B. (1999). Factors controlling the growth of polyelectrolyte multilayers. *Macromolecules*, *32* (24), 8153-8160.

Edwards, R, Harding, KG. (2004). Bacteria and wound healing. *Curr. Opin. Infect. Dis.*, *17* (2), 91–96.

Engel, L. S., Hill, J. M., Caballero, A. R., Green, L. C., O'Callaghan, R. J. (1998) Protease Iv, a unique extracellular protease and virulence factor from *Pseudomonas*

aeruginosa. J. Biol. Chem., *273* (27), 16792-16797.

Etrych, T., Boustta, M., Leclercq, L. Vert, M. (2006). Release of polyanions from polyelectrolyte complexes by selective degradation of the polycation. *J. Bioactive Compatible Polymers.*, *21* (2), 89-105.

Everhart, D. S. (*Ed.* Holmberg, K.) (2002). Self-assembling monolayers: alkane thiols on gold. Handbook of applied surface and colloid chemistry. *Wiley, Chichester*, p. 99-116.

Flattau, A., Schiffman, J., Lowy, F. D., Brem, H. (2008). Antibiotic.resistant gram-negative bacteria in deep tissue cultures. *Int. Wound J.*, *5* (5), 599-600.

Fleer, G. J., Cohen Stuart, M. A., Scheutjens, J. M. H. M., Cosgrove, T., Vincent, B. (1993). Polymers at interfaces. *Chapman & Hall, London, UK*, p. 18, 30.

Gergely, C., Bahi, S., Szalontai, B., Flores, H., Schaaf, P., Voegel, J. C., Cuisinier, F. J. G. (2004). Human serum albumin self-assembly on weak polyelectrolyte multilayer films structurally modified by pH changes. *Langmuir*, *20* (13), 5575-5582.

Gilbert, P., Moore, L. E. (2005). Cationic antiseptics: diversity of action under a common ephitet. *J. Appl. Microbiol.*, *99,* 703-715.

Gordon, M. D., Gottschlich, M. M., Helvig, E. I., Marvin, J. A., Richard, R. L. (2004). Review of evidence-based practice for the prevention of pressure sores in burn patients. *J. Burn Care Rehabil.*, *25* (5), 388–410.

Greener, B., Hughes, A. A., Bannister, N. P., Douglass, J. (2005). Proteases and pH in chronic wounds. *J. Wound Care*, *14* (2), 59–61.

Gu, H., Ho, P. L., Tong, E., Wang, L., Xu, B. (2003) Presenting Vancomycin on nanoparticles to enhance antimicrobial activities. *Nano Lett. 3* (9), 1261-1263.

Gurunathan, S., Woong Han, J., Kwon, D. N., Kim, J. H. (2014) Enhanced antibacterial and anti-biofilm activities of silver nanoparticles against Gram-negative and Gram-positive bacteria. *Nanoscale Res. Lett. 9* (1), 1-17.

Halthur, T. J., Elofsson, U. M. (2004-I). Multilayers of charged polypeptides as studied by in situ ellipsometry and quartz crystal microbalance with dissipation. *Langmuir*, *20* (5), 1739-1745.

Halthur, T. J., Claesson, P. M., Elofsson, U. M. (2004-II). Stability of polypeptide multilayers as studied by in situ ellipsometry: Effects of drying and post-buildup changes in temperature and pH. *J. Am. Chem. Soc.*, *126* (51), 17009-17015.

Halthur, T. J., Claesson, P. M., Elofsson, U. M. (2006). Immobilization of enamel matrix derivate protein onto polypeptide multilayers. Comparative in situ measurements using ellipsometry, quartz crystal microbalance with dissipation, and dual-polarization interferometry. *Langmuir*, *22* (26), 11065-11071.

Heck, L. W., Darby, W. L., Hunter, F. A., Bhown, A., Miller, E. J., Bennett, J. C. (1985). Isolation, characterization, and amino-terminal amino acid sequence analysis of human neutrophil elastase from normal donors. *Anal. Biochem.*,*149* (1), 153-162.

Hess, C. T. (2004). Putting the squeeze on venous ulcers. *Nursing*, *34* (Suppl Travel), 8–13.

Holmberg, K., Jönsson, B., Kronberg, B., Lindman B. (2003). Surfactants and polymers in aqueous solution. 2nd ed. *John Wiley & Sons, Ltd, West Sussex, England*, p. 207.

Honeyman A. L., Friedman, H., Bendinelli, M. (2002). *Staphylococcus aureus* infection and

disease. Kluwer Academic Publishers, New York, ISBN: 0-306-46848-4.

Hsieh, C. Y., Tsai, S. P., Wang, D. M., Chang, Y. N., Hsieh, H. J. (2005). Preparation of γ-PGA/chitosan composite tissue engineering matrices.*Biomaterials*, *26* (28), 5617-5623.

Höök, F., Rodahl, M., Brzezinski, P., Kasemo, B. (1998). Energy dissipation kinetics for protein and antibody-antigen adsorption under shear oscillation on a quartz crystal microbalance. *Langmuir*, *14* (4), 729-734.

Höök, F., Kasemo, B., Nylander, T., Fant, C., Sott, K., Elwing, H. (2001-I). Variations in coupled water, viscoelastic properties, and film thickness of a Mefp-1 protein film during absorption and cross-linking: a quartz crystal microbalance with dissipation monitoring, ellipsometry, and surface plasmon resonance study. *Anal. Chem.*, *73* (24), 5796-5804.

Höök, F., Kasemo, B., Nylander, T., Fant, C., Sott, K., Elwing, H. (2001-II). Missing mass' effect in biosensor's QCM applications. *Biosens. Bioelectron.*, *73* (24), 5796-5804.

Höök, F., Vörös, J., Rodahl, M., Kurrat, R., Böni, P., Ramsden, J. J., Textor, M., Spencer, N. D., Tengvall, P., Gold, J., Kasemo, B. (2002). A comparative study of protein adsorption on titanium oxide surfaces using in situ ellipsometry, optical waveguide lightmode spectroscopy, and quartz crystal microbalance/dissipation. *Colloids Surf. B*, *24* (2), 155-170.

Höök, F., Kasemo, B. (2007). Piezoelectric Sensors: The QCM-D technique for probing biomacromolecular recognition reactions. *Springer Berlin Heidelberg*, p. 425-447.

Ikeda, T., Ledwith, A., Bamford, C. H., Hann, R. A. (1984). Interaction of a polymeric biguanide biocide with phospholipid membranes. *BBA Biomembranes*, *768* (1), 57-66.

Janeesh, P. A., Sami, H., Dhanya, C. R., Sivakumar, S., Abraham, A. (2014) Biocompatibility and genotoxicity studies of polyallylamine hydrochloride nanocapsules in rats. *RSC Adv.*, *4* (47) 24484-24497.

Jarrod, S., Aksone, N. (2011). Assessment of microcirculation and the prediction of healing in diabetic foot ulcers. In: Topics in the prevention, treatment and complications of type 2 diabetes. Ed. Zimering, M. B., InTech, New York, 2011, Chapter 11.

Jensen, K., Østergaard, P. R., Wilting, R., Lassen, S. F. (2010). Identification and characterization of a bacterial glutamic peptidase. *BMC Biochemistry*, *11* (47), 1-12.

Jessel, N., Atalar F., Lavalle, P., Mutterer, J., Decher, G., Schaaf, P., Voegel, J.-C., Ogier, J. (2003). Bioactive coatings based on a polyelectrolyte multilayer architecture functionalized by embedded proteins. *Adv. Mater.*, *15* (9), 692-695.

Kaehn,, K. (2010). Polihexanide: A safe and highly effective biocide. *Skin Pharmacol. Physiol.*, *23* (suppl. 1), 7–16.

Kell, A. J., Stewart, G., Ryan, S., Peytavi, R., Boissinot, M., Huletsky, A., Bergeron, M. G., Simard, B. (2008) Vancomycin-modified nanoparticles for efficient targeting and preconcentration of Gram-positive and Gram-negative bacteria. *ACS Nano 2* (9), 1777-1788.

Kickelbick, G. (2007). Hybrid materials: synthesis, characterization, and applications. *Wiley, Weinheim, Germany*, p. 107.

Kirketorp-Møller, K., Zulkowski, K., James, G. (Eds.: Bjarnsholt T., Moser C., Høiby N.) (2011). Biofilm Infections: Chronic wound colonization, infection, and biofilms. *Springer, New York*, ISBN: 978-1-4419-6083-2, chapter 2.

Knag, M., Sjöblom, J., Oye, G., Gullbrandsen, E. (2004). A quartz crystal microbalance study

of the adsorption of quarternary ammonium derivates on iron and cementite. *Colloids Surf. A*, *250* (1-3), 269-278.

Korkmaz, B., Hajjar, E., Kalupov, T., Reuter, N., Brillard-Bourdet, M., Moreau T., Juliano, L., Gaunthier, F. (2007). Influence of charge distribution at the active site surface on the substrate specificity of human neutrophil protease 3 and elastase. *J. Biol. Chem.*, *282* (3), 1989-1997.

Kramer, A., Roth, B., Müller, G., Rudolph, P., Klocker, N. (2004). Influence of the antiseptic agents polyhexanide and octenidine on FL cells and on healing of experimental superficial aseptic wounds in piglets. A double-blind, randomized, stratified, controlled, parallel-group study. *Skin Pharmacol Physiol.*, *17* (3), 141-146.

Kuhn, B. A., Coulter, S. J. Balancing ulcer cost and quality equation. (1992). *Nurs. Econ.*, *10* (5), 353–359.

Landis, S. J. (2008). Chronic wound infection and antimicrobial use. *Adv. Skin Wound Care*, *54* (3), 30–34.

Lavalle, P., Gergely, C., Cuisinier, F. J. G., Decher, G., Schaaf, P., Voegel, J. C., Picart, C. (2002). Comparison of the structure of polyelectrolyte multilayer films exhibiting a linear and an exponential growth regime: an in situ atomic force microscopy study. *Macromol.*, *35* (11), 4458-4465.

Leid, J. G., Willson, C. J., Shirtliff, M. E., Hassett, D. J., Parsek, M. R., Jeffers, A. K. (2005). The exopolysaccharide alginate protects *Pseudomonas aeruginosa* biofilm bacteria from IFN-gamma-mediated macrophage killing. *J. Immunol.*, *175* (11), 7512–7518.

Levine, D. P. (2006). Vancomycin: a history. *Clin. Infect. Dis. 42*, S5-12.

Li, B., Jiang, B., J., Boyce, B. M., Lindsey, B. A. (2009). Multilayer polypeptide nanoscale coatings incorporating IL-12 for the prevention of biomedical device-associated infections. *Biomaterials*, *30*, 2552-2558.

Li, H., Ogle, H., Jiang, B., Hagar, M., Li, B. (2010). Cefazolin embedded biodegradable polypeptide nanofilms promising for infection prevention: A preliminary study on cell responses. *J. of Orthopaedic Research*, *28* (8), 992-999.

Lindstedt, M., Allenmark, S., Thompson, R. A. and Edebo, L. (1990). Antimicrobial activity of betaine esters, quaternary ammonium amphiphiles which spontaneously hydrolyse into nontoxic components. *Antimicrob. Agents Chemother.*, *43*, 1949-1954.

Lvov, Y., Haas, H., Decher, G., Möhwald, H., Michailov, A., Mtchedlishvily, B., Morgunova, E., Vainshtain, B. (1994). Successive deposition of alternate layers of polyelectrolytes and a charged virus. *Langmuir*, *10*, 4232-4236.

Malmsten, M. (2003). Biopolymers at interfaces. Second ed., revised and expanded. *Marcel Dekker, Inc. New York*, ISBN: 0-8247-0863-6, p. 14-15.

Marchenko, I., Yashchenok, A., Borodina, T., Bukreeva, T., Konrad, M., Möhwald, H., Skirtach, A. (2012). Controlled enzyme-catalyzed degradation of polymeric capsules template on $CaCO_3$: influence of the number of LbL layers, conditions of degradation, and disassembly of multicompartments. *J. Control. Rel.*, *162* (3), 599-605.

Mendelsohn, J. D., Yang, S. Y., Hiller, J., Hochbaum, A. I., Rubner, M. F. (2003). Rational design of cytophilic and cytophobic polyelectrolyte multilayer thin films. *Biomacromol.*, *4*, 96-106.

Méndez Garza, J., Jessel, N., Ladam, G., Dupray, V., Muller, S., Stoltz, J. F., Schaaf, P.,

Voegel, J.-C, Lavalle, P. (2005). Polyelectrolyte multilayers and degradable polymer layers as multicompartment films. *Langmuir.,* 21 (26), 12372-12377.

Nagy, M. (2010). Thermodynamic study of aqueous solutions of polyelectrolytes of low and medium charge density without added salt by direct measurement of osmotic pressure. *J. Chem. Thermodyn.*, *42* (3), 387-399.

Nemoto, T. K., Ohara-Nemoto, Y., Ono, T., Kobayakawa, T., Shimoyama, Y., Kimura, S., Takagi, T. (2008). Characterization of the glutamyl endopeptidase from *Staphylococcus aureus* expressed in *Escherichia coli*. *FEBS Journal*, *275*, 573-587.

Netz, R. R., Andelman, D. (2007). Encyclopedia of electrochemistry: Polyelectrolytes in solution and at surfaces. *Wiley-VCH Verlag GmbH & Co. KGaA, Weinheim*, ISBN: 9783527610426, p. 282.

Nitzan, D. W., Nitzan, U., Dan, P., Yedgar, S. (2001) The role of hyaluronic acid in protecting surface-active phospholipids from lysis by exogeneous phospholipase A_2. *Rheumatol.*, *40* (3), 336-340.

Ohara-Nemoto, Y., Ikeda, Y., Kobayashi, M., Sasaki, M., Tajika, S., Kimura, S. (2002). Characterization and molecular cloning of a glutamyl endopeptidase from *Staphylococcus epidermidis*. *Microb. Pathog.*, *33*, 33-41.

Ono, T., Ohara-Nemoto, Y., Shimoyama, Y., Okawara, H., Kobayakawa, T., Baba, T. T., Kimura, S., Nemoto, T. K. (2010). Amino acid residues modulating the activities of staphylococcal glutamyl endopeptidases. *Biol. Chem.*, *391* (10), 1221-1232.

Oskarsson, H., Holmberg, K. (2006). Adsorption of ethoxylated cationic surfactants on self-assemled monolayers of alkanethiols on gold using surface plasmon resonance detection. *J. Colloid Interface Sci.*, *301* (2), 360-369.

Palamà, I. E., Musarò, M., Coluccia, A. M. I., D'Amone, S., Gigli, G. (2011). Cell uptake and validation of novel PECs for biomedical applications. *J. Drug Deliv.*, *2011*, ID 203676, 7 pages.

Paulus, W. (2004). Directory of microbiocides for the protection of materials. *Kluwer Academic Publishers, The Netherlands*, ISBN 1-4020-2817-2, p. 727-728.

Percival, S. L., Woods, E., Nutekpor, M., Bowler, P., Radford, A., Cochrane, C. (2008). Prevalence of silver resistance in bacteria from diabetic foot ulcers and efficacy of silver-containing wound dressings. *OWM*, *21* (11), 531-540.

Pham, C. T. N. (2006). Nautrophil serine proteases: specific regulators of inflammation. *Nat. Rev. Immunol.*, *6*, 541-550.

Picart, C., Lvalle, Ph., Hubert, P., Cuisinier, F. J. G., Decher, G., Scaaf, P., Voegel, J. C. (2001). Buildup mechanism for poly(L-lysine)/hyaluronic acid films onto a solid surface. *Langmuir*, *17*, 7414-7424.

Pilbat, A. M., Ball, V., Schaaf, P., Voegel, J. C., Szalontai, B. (2006). Partial poly(glutamic acid) - poly(aspartic acid) exchange in layer-by-layer polyelectrolyte films. Structural alterations in the three-component architectures. *Langmuir*, *22* (13), 5753-5759.

Poon, Z., Lee, J.B., Morton, S.W., Hammond, P.T. (2011). Controlling in vivo stability and biodistribution in electrostatically assembled nanoparticles for systemic delivery. *Nano Lett. 11* (5) 2096-2103.

Prasad, L., Leduc, Y., Hayakawa, K., Delbaere, T. J. (2004). The structure of a universally employed enzyme: V8 protease from *Staphylococcus aureus*. *Acta Cryst.*, *D60*, 256-259.

Reynolds, P. E. (1989) Structure, biochemistry and mechanism of action of glycopeptides antibiotics. *Eur. J. Clin. Microbiol. Infect. Dis.* *8* (11), 943-950.

Richert, L., Lavalle, Ph., Senger, B., Stoltz, J. F., Schaaf, P., Voegel, J. C., Picart, C. (2002). Cell interactions with polyelectrolyte multilayer films. *Biomacromolecules*, *3* (6), 1170-1178.

Richert, L., Arntz, Y., Schaaf, P., Voegel, J.-C., Picart, C. (2004). pH dependent growth of poly(L-lysine)/poly(L-glutamic) acid multilayer films and their cell adhesion properties. *Surf.. Sci.*, *570* (1-2), 13-29.

Rodahl, M., Höök, F., Krozer, A., Brzezinski, P., Kasemo, B. (1995). Quartz crystal microbalance setup for frequency and Q-factor measurements in gaseous and liquid environments. *Rev. Sci. Instr.*, *66* (7), 3924-3930.

Rodahl, M., Kasemo, B. (1996). A simple setup to simultaneously measure the resonant frequency and the absolute dissipation factor of a quartz crystal microbalance. *Rev. Sci. Instrum.*, *67* (9), 3238-3241.

Sauerbrey, G. (1959). The use of quartz oscillators for weighing thin layers and for microweighing. *Z. Phys.*, *155*, 206-222.

Schrøder-Leiros, H., Brandsdal, B. O., Andersen, O. A., Os, V., Leiros, I., Helland, R., Otlewski, J., Willassen, N. P., Smalås, A. O. (2004). Trypsin specificity as elucidated by LIE calculations, X-ray structures, and association constant measurements. *Protein Science*, *13*, 1056-1070.

Sen, C. K., Gordillo, G. M., Roy, S., Kirsner, R., Lambert, L., Hunt, T. K., Gottrup, F., Gurtner, G. C., Longaker, M. T. (2009). Human skin wounds: a major and snowballing threat to public health and the economy. *Wound Repair Regen*, *17* (6), 763–771.

Shukla, A., Fleming, K. E., Chuang, H. F., Chau, T. M., Loose, C. R., Stephanopoulos, G. N., Hammond, P. T. (2010). Controlling the release of peptide antimicrobial agents from surfaces. *Biomaterials*, *31* (8), 2348-2357.

Siedle, B., Hrenn, A., Merfort, I. (2007). Natural compounds as inhibitors of human neutrophil elastase. *Planta Med.*, *73*, 401-420.

Sinha, S., Watorek, W., Karr, S., Giles, J., Bode, W., Travis, J. (1987). Primary structure of human neutrophil elastase. *Proc. Natl. Acad. Sci.*, *84*, 2228-2232.

Sorensen, S. B., Sorensen, T. L., Breddam, K. (1991). Fragmentation of proteins by *S. aureus* strain V8 protease: Ammonium bicarbonate strongly inhibits the enzyme but does not improve the selectivity for glutamic acid. *FEBS Lett.*, *294* (3), 195–197.

Suchy, M., Linder, M. B., Tammelin, T., Campbell, J. M., Vuorinen, T., Kontturi, E. (2011). Quantitative assessment of the enzymatic degradation of amorphous cellulose by using a quartz crystal microbalance with dissipation monitoring. *Langmuir*, *27* (14), 8819-8828.

Sukhorukov, G. B., Möhwald, H., Decher, G., Lvov, Y. M. (1996). Assembly of polyelectrolyte multilayer films by consecutively alternating adsorption of polynucleotides and polycations. *Thin Solid Films*, *284-285*, 220-223.

Szarpak, A., Pignot-Paintrand, I., Nicolas, C., Picart, C., C., Auzély-Velty, R. (2008). Multilayer assembly of hyaluronic acid/poly(allylamine): Control of the buildup for the production of hollow capsules. *Langmuir*, *24*, 9767-9774.

Szarpak, A., Cui, D., Dubreuil, F., De Geest, B. G., De Cock, L. J., Picart, C., Auzély-Velty, (2010). R. Designing hyaluronic acid-based layer-by-layer capsules as a carrier for

intracellular drug delivery. *Biomacromolecules*, *11*, 713-720.

Takahashi, A., Kato, N., Nagasawa, M. (1970). The osmotic pressure of polyelectrolyte in neutral salt solutions. *J. Phys. Chem.*, *74*, 944-946.

Thompson, R. A., Allenmark, S. (1989). Effects of molecular association on the rates of hydrolysis of long-chain alkyl betainates. *Acta Chem. Scand.*, *43*, 690-693.

Todar, K. (2012). Todar's online textbook of bacteriology, Chapter: *Staphylococcus aureus* and Staphylococcal Disease. www.textbookofbacteriology.net

Tompkins, H. G., Irene, E. A. (2005). Handbook of Ellipsometry. *William Andrew Inc. and Springer-Verlag, Norwich, NY and Heidelberg, Germany.*

Ulman, A. (1996). Formation and structure of self-assembled monolayers. *Chem. Rev.*, *96* (4), 1533-1554.

Velnar, T., Bailey, T., Smrkolj, V. (2009). The wound healing process: an overview of the cellular and molecular mechanisms. *J. Int. Med. Res. 37* (5) 1528-1542.

Vogt, B. D., Lin, E. K., Wu, W. L., White, C. C. (2004). Effect of film thickness on the validity of the Sauerbrey equation for hydrated polyelectrolyte films. *J. Phys. Chem. B*, *108* (34), 12685-12690.

Voinova, M. V., Rodahl, M., Jonson, M., Kasemo, B. (1999). Viscoelastic acoustic response of layered polymer films at fluid-solid intefaces: continuum mechanics approach. *Phys. Scr.*, *59* (5), 391-396.

Voinova, M. V., Jonson, M., Kasemo, B. (2002). Missing mass' effect in biosensor's QCM applications. *Biosens. Bioelectron.*, *17* (10), 835-841.

Volodkin, D. V., Petrov, A. I., Prevot, M., Sukhorukov, G. B. (2004). Matrix polyelectrolyte microcapsules:New system for macromolecule encapsulation. *Langmuir*, *20*, 3398-3406.

Vuong, C., Voyich, J. M., Fischer, E. R., Braughton, K. R., Whitney, A. R., Deleo, F. R., Otto, M. (2004). Polysaccharide intercellular adhesin (PIA) protects *Staphylococcus epidermidis* against major components of the human innate immune system. *Cell. Microbiol.*, *6* (3), 269–275.

Wang, L., Wang, X., Xu, M., Sun, J. (2008). Layer-by-layer assembled microgel films with high loading capacity: reversible loading and release of dyes and nanoparticles. *Langmuir*, *24* (5), 1902-1909.

Wilderman, P. J., Vasil, A. I., Johnson, Z., Wilson, M. J., Cunliffe, H. E., Lamont, I. L., Vasil, M. L. (2001) Characterization of an endoprotease (PrpL) encoded by a PvdS-regulated gene in *Pseudomonas aeruginosa*. *Infect. Immun.*, *69* (9), 5385-5394.

Wolcott, R. D., Rumbaugh, K. P., James, G., Schultz, G., Phillips, P., Yang, Q., Watters, C., Stewart, P. S., Dowd, S. E. (2010) Biofilm maturity studies indicate sharp debridement opens a time-dependent therapeutic window. *J. Wound Care 19* (8), 320-328.